Atmos. Chem. Phys. Discuss., doi:10.5194/acp-2016-942, 2016
Manuscript under review for journal Atmos. Chem. Phys.
Published: 24 November 2016

Atmospheric Chemistry and Physics Discussions
Open Access

Implications on atmospheric dynamics and the effect on black carbon transport into the Eurasian Arctic based on the choice of land surface model schemes and reanalysis data in model simulations with WRF.

Carolina Cavazos Guerra[1], Axel Lauer[2], Andreas B. Herber[3], Tim M. Butler[1], Annette Rinke[4], Klaus Dethloff[4]

[1]. Institute for Advanced Sustainability Studies (IASS), Potsdam, Germany.

[2]. Deutsches Zentrum für Luft- und Raumfahrt (DLR), Institut für Physik der Atmosphäre, Oberpfaffenhofen, Germany.

[3]. Alfred Wegener Institute, Helmholtz Centre for Polar and Marine Research, Research Unit Bremerhaven, Germany.

[4]. Alfred Wegener Institute, Helmholtz Centre for Polar and Marine Research, Research Unit Potsdam, Germany.

Correspondence to: Carolina Cavazos-Guerra (carolina.cavazosguerra@iass-potsdam.de)

Abstract

A realistic simulation of physical and dynamical processes in the Arctic atmosphere and its feedbacks with the surface conditions is still a challenge for state-of-the-art Arctic climate models. This is of critical importance because studies of, for example, transport of pollutants from middle latitudes into the Arctic rely on the skill of the model in correctly representing atmospheric circulation including the key mechanisms and pathways of pollutant transport. In this work the performance of the Weather Research and Forecast model (WRF) with two land surface model schemes (Noah and NoahMP) and two reanalysis data sets for creation of lateral boundary conditions (ERA-interim and ASR) is evaluated focusing on meteorological surface properties and atmospheric dynamics. This includes the position and displacement of the polar dome and other features characterizing atmospheric circulation associated to sea ice maxima/minima extent within the Eurasian Arctic. The model simulations analyzed are carried out at 15-km horizontal resolution over a period of five years (2008 to 2012). The WRF model simulations are evaluated against surface meteorological data from automated weather stations and vertical profiles from radiosondes. Results show that the model is able to reproduce the main features of the atmospheric dynamics and vertical structure of the Arctic atmosphere reasonably well. The influence of the choice of the reanalyses used as initial and lateral boundary condition and of the LSM on the model results is complex and no combination is found to be clearly superior in all variables analyzed. The model results show that a more sophisticated formulation of land surface processes does not necessarily lead to significant improvements in the model results. This suggests that other factors such as the decline of the Arctic sea ice, stratosphere-troposphere interactions, atmosphere-ocean interaction, and boundary layer processes are also highly important and can have a significant influence on the model results.

The "best" configuration for simulating Arctic meteorology and processes most relevant for pollutant transport (ASR + NoahMP) is then used in a simulation with WRF including aerosols and chemistry (WRF-Chem) to simulate black carbon (BC) concentrations in and around the Arctic and to assess the role of the modeled atmospheric circulation in the simulated BC concentrations inside the Arctic domain. Results from simulations with chemistry are evaluated against aerosol optical depth from several Aeronet stations and BC concentrations and particle number concentrations from several stations from the EBAS database. The results with WRF-Chem show a strong dependency of the simulated BC concentration on the modeled meteorology and the transport of the pollutants around our domain. The results also show that biases in the modeled BC concentrations can also be related to the emission data. Significant improvements of the models and of our understanding of the impact of anthropogenic BC emissions on the Arctic strongly depends on the availability of suitable, long-term observational data of concentrations of BC and particulate matter, vertical profiles of temperature and humidity and wind.

1 Introduction

The Arctic atmosphere is often characterized by a stable boundary layer and strong near-surface temperature inversions, which limit turbulent mixing and vertical transport due to the combined effects of efficient cooling by upward long wave radiation and reflection of short wave at the surface as a result of the high sea ice concentration and relatively flat and homogeneous surface in the inner part of the Arctic Ocean. This negative radiation budget at the surface is amplified by the typically low atmospheric moisture and cloud free conditions (Anderson and Neff, 2008). This effect is most pronounced during winter when there is little or no sunlight and the surface is frequently covered by snow or ice (Bradley et al., 1992). Consequently, a 'dome' forms that is characterized by low and constant potential temperatures and isolates the Arctic lower troposphere from the rest of the atmosphere by acting as a barrier (the so-called Arctic front). The Arctic front separates the cold Arctic air from warmer air in the south and can reach as far south as 40°N during the coldest periods of the year (Stohl, 2006). The pronounced seasonal cycle of these atmospheric features strongly determines transport mechanisms and pathways of pollutants into the Arctic (Schnell, 1984; Sharma et al., 2006).

Sea ice is part of a complex system that acts as an interface between the atmosphere and the ocean: the ice inhibits vertical heat transfer between the atmosphere and the ocean, and contributes to the ice-albedo feedback mechanism. The Arctic summer sea ice extent which has been observed over the last 30 years by satellites (Meier et al, 2006) has an effect on the atmospheric temperature gradient in the lower atmosphere (Serreze et al., 2000). For example, a larger sea ice-free area results in an increase in absorbed heat in the upper ocean, leading in in turn to the increase in the near-surface temperature maximum (Jackson et al. 2010). This pattern affects atmospheric circulation by modifying weather patterns in the Arctic and beyond, an effect also referred as the Arctic amplification (e.g. Screen and Simmonds, 2010; Cohen, et al., 2014). These changes in atmospheric circulation connected to the decline of Arctic sea ice and changes in continental snow-cover may also disturb temperature and precipitation patterns and increase the likelihood of extreme weather events in mid-latitudes (Overland and Wang, 2010; Jaiser, et al., 2012; Handorf et al., 2015). The Arctic is usually dominated by low pressure in winter forming a "Polar Vortex" of counter-clockwise circulating winds around the Arctic. In a warming Arctic, high pressure replaces the low pressure, weakening the Polar Vortex and reversing the circulation in which cold air flows southwards and warm air moves poleward (Honda, et al 2009; Petoukhov and Semenov, 2010). This happened in winter 2009/2010 leading to unusually cold and snowy winter conditions in China, Eastern Asia, the eastern United States and Europe, whereas West Greenland and the Bering Strait experienced anomalous warm temperatures (Seager et al., 2010).

The pronounced seasonal cycle of the extent of the Arctic front plays a key role in the transport of black carbon (BC) and other pollutants from source regions in mid-latitudes including Asia, Russia, North America and North Europe into the Arctic. The maximum advection of pollution into the Arctic occurs usually in winter and early spring (*i.e.*, the 'Arctic haze' season) and the minimum in summer when the Arctic aerosol is diminished by clouds and precipitation. In winter (particularly in January), northern Eurasia is one of the major source regions for the Arctic pollution. Polluted air masses from densely populated areas over East-Asia and North America are typically too warm and moist to directly penetrate the polar dome, but they can descend into the Arctic middle or upper troposphere creating the Arctic haze (Stohl, 2006).

An important aim of many Arctic modeling studies is to improve our understanding of the causes, governing mechanisms, and effects of Arctic amplification in order to better characterize the relevant physical processes in the Arctic ocean–atmosphere–cryosphere system (in particular atmospheric boundary-layer processes). However, the complexity of these processes and their interactions are still a challenge for modeling the Arctic (Vihma et al., 2014) leading to a large spread in model results and a large sensitivity to a wide set of parameters regarding model configuration and initialization.

Model biases in global climate models (GCMs) used for present-day and future climate simulations are partly related to the horizontal and vertical resolution (e.g. Duffy et al., 2003; Wehner et al., 2010). Coarse horizontal resolution, for example, can lead to the overestimation in sensible heat fluxes (Schmittner et al., 2002). In recent years Regional Climate Models (RCMs) have gained popularity as they are computationally less expensive and are capable of capturing mesoscale coupled processes and regional climatic evolution due to the ability to run at very high spatial and temporal resolutions (Dethloff et al., 1996).

Model parameterizations play an important role in representing the vertical stratification and atmosphere–surface energy exchange in model simulations (Dethloff et al., 2001). For example, some differences in regional model simulations can be attributed to the boundary layer and surface parameterizations used, which result in surface flux differences, and to the lateral moisture forcing, both of which affect moisture availability in the atmosphere (Rinke et al., 2000). Therefore, it is critical to choose schemes suitable for the relevant Arctic processes as the application of non-suitable schemes may introduce biases into the model outputs (Misenis and Zhang, 2010). This is particularly relevant for Arctic studies as model parameterizations are typically developed and tested for mid-latitude conditions which may not be suitable for use in the Arctic. Optimizing the model configuration for Arctic simulations is also needed in order to be able to reduce the uncertainties in high-resolution projections of future Arctic climate and to be able to better assess the impacts of climate change over the Arctic and beyond. For example, Land Surface Models (LSMs) implemented in climate models (designed to calculate processes at the surface-atmosphere interface) play a critical role in the representation of the heat budget.

Data used as initial and lateral boundary conditions also play an important role in the results of a RCM as the quality of the data used have direct implications on the quality of the model outputs (Denis et al., 2003; Diaconescu et al., 2007). However, the quality of a reanalysis may also vary regionally in some variables, especially in areas where observations are sparse. Despite these limitations, reanalysis data provide gridded, self-consistent datasets suitable for model evaluation and to perform a comprehensive examination of climate variability (Trenberth et al., 2008).

In addition to these challenges for numerical modeling of the Arctic atmosphere, deficiencies in the treatment of aerosols and clouds may reduce the accuracy in climate model projections (Overland and Wang, 2013). The wide spread of model results for the distribution of aerosols over the Arctic can be attributed to, for instance, differences in emissions, chemistry and transport schemes (Shindell et al., 2008). Even though simulations of BC concentrations in the Arctic from recent studies are in better agreement with observations, the amplitude of the seasonal cycle of BC is still underestimated by most models (Eckardt et al., 2015). Because of the strong dependency of the radiative forcing by aerosols on the surface albedo (Haywood and Shine, 1997), uncertainties in the surface albedo in the models translate directly into uncertainties in estimates of the absorption of solar radiation by BC over high albedo surfaces (Myhre et al., 2009).

In this work we assess the performance of the Weather and Research Forecasting (WRF) model in representing surface/atmosphere dynamics depending on the selection of the Land Surface Model (LSM) parameterization and reanalysis datasets for initialization and provision of lateral boundary conditions (ERA-Interim and Arctic System Reanalysis). The meteorological study is conducted over a five year period (2008-2012) for two seasons: February, March and April (hereafter FMA) and July, August and September (hereafter JAS) coinciding with the maximum and minimum sea ice extent in the region, respectively, within the Eurasian Arctic region. In particular, we assess the magnitude of model biases on the surface meteorology including air temperature, wind speed, geopotential, the evolution of the planetary boundary layer (PBL) and the position of the Arctic dome over the Eurasian Arctic. We then investigate the implications of these model biases on the atmospheric circulation influencing concentrations of black carbon in and advected towards the Eurasian Arctic by comparing results for aerosol optical depth (AOD) and concentrations of black carbon from corresponding simulations with WRF-Chem with observations. The selected case studies using the WRF-Chem are conducted for periods characterized by the minimum (warm period) and maximum (cold period) observed tropospheric concentrations of BC over the Arctic north of 66°N (Stohl, 2006).

The paper is organized as follows: In section 2, the model configuration, experimental design and observational data used for model validation are described. In section 3 we present the analysis of biases between model outputs and observational data for the set of simulations with the WRF model focusing on meteorology, followed by results from selected case studies using a model configuration including air chemistry and aerosols (WRF-Chem). The discussion and conclusions are presented in section 4.

2 Methodology

2.1. Model description and simulations

2.1.1 The weather research and forecasting model (WRF)

For the sensitivity analyses we use the Advanced Research version 3.7.1 of the weather research and forecasting model (WRF). WRF is a mesoscale forecast model and assimilation system developed by the National Center for Atmospheric Research (NCAR) together with several partners. More details about the development of WRF can be found in Michalakes et al. (2005). The WRF model is designed for a wide range of applications from idealized research to operational forecasting, with an emphasis on horizontal grid sizes in the range of 1–10 km. Several physics options in the form of different packages are available for relevant physical processes including microphysics of clouds and precipitation, cumulus convection, planetary boundary layer and surface layer physics, turbulence and diffusion and radiation (longwave and shortwave). All of these schemes consist of solver-dependent routines approximating or parameterizing physical processes that are too complex or too computationally costly to be explicitly represented (Skamarock, 2005).

The model physics packages used in this study for the meteorological WRF model set up (also defined in Table 1) are: (1) the atmospheric surface layer scheme which calculates momentum and heat fluxes at the surface uses the MM5 similarity scheme based on Monin-Obukhov with Carslon-Boland viscous sub-layer and standard similarity functions from look-up tables (Beljaars,1994), (2) convective processes following the Grell 3D parameterization, a multi-closure, multi-parameter ensemble method which is an improved version of the Grell-Devenyi ensemble scheme for horizontal grid sizes larger than 10 km (Grell and Devenyi, 2002), (3) the PBL (Planetary Boundary Layer) parameterization implemented is the non-local Yonsei University (YSU) scheme (Hong, 2010) which calculates atmospheric tendencies of temperature, moisture with clouds, and horizontal momentum (4) Lin et al. (1983) cloud microphysics including cloud ice, snow and graupel processes, (5) radiative processes are parameterized using the Rapid Radiative Transfer Model for Long Wave (LW) radiation (Mlawer et al., 1997) and the Dudhia (1989) scheme for short wave (SW) radiation, and finally (6) the land-surface parameterization (hereafter LSM) which characterizes heat, moisture and radiation fluxes at the surface and resulting feedbacks with the atmosphere. Sensitivity analyses were conducted using two available LSM schemes, the Unified Noah Land Surface Model (Chen and Dudhia, 2001) and the Noah–MP Land Surface Model (Niu et al., 2011; Yang et al., 2011). A more detailed description of both LSM schemes is given in the next section.

Land Surface Models (LSMs)

LSMs simulate surface/atmosphere dynamics and the land surface variability by including the relevant land surface/hydrology processes. The variables resolved in the LSM parameterization interact directly with other physical parameterizations in WRF such as cloud microphysics and cumulus schemes, radiation schemes and certain land and ocean variables that impact the vertical transport (surface layer) and the PBL. LSMs also calculate sea ice processes affecting ice temperature, skin temperature, snowpack water content, snow depth, and surface energy (note that LSMs in WRF currently do not include sea ice generation, melting, and change in thickness).

Some modeling studies (e.g. Misenis and Zhang, 2010) have suggested that there is a higher sensitivity of WRF to the LSM schemes than to PBL schemes for simulating standard meteorological variables including surface temperature, relative humidity and wind vectors, due to differences in surface fluxes. This fact may affect performance of the atmospheric model over the Arctic. Thus, we performed sensitivity studies with both LSM schemes to investigate their strengths and limitations for Arctic applications and the implications in reproducing important meteorological variables. The experimental design of the simulations performed in this work is well detailed in section 2.1.4 and also shown in Table 1b.

The two tested LSM schemes used in this work are the Noah Land Surface Model (Noah LSM) developed by the Oregon State University and a more detailed and updated version, the Noah Multi-Physics (NoahMP). The Noah scheme calculates the soil temperature, as well as the soil and canopy moisture in four layers (10, 30, 60, and 100 cm thick) and includes fractional snow cover and frozen soil physics (Chen and Dudhia, 2001; Ek and Mitchell, 2003). The surface skin temperature is calculated with a single linearized surface energy balance equation representing the combined ground-vegetation surface. Soil temperature is calculated solving the thermal diffusion equation, soil moisture is predicted using the Richards equation (Richards, 1931). Known limitations of the Noah LSM model include the tendency of the Noah scheme to produce too little snow cover during spring (e.g., Barlage et al., 2010), significant biases in surface temperature due to structural limitations when heterogeneities exist at the surface (Miguez-Macho et al., 2008; Fan et al., 2007) and larger seasonal variations in snow water equivalent compared to other LSM schemes (Chen et al., 2014). As a side note, one of the reasons for using the latest version of WRF 3.7.1 is due to the fact that in

Atmos. Chem. Phys. Discuss., doi:10.5194/acp-2016-942, 2016
Manuscript under review for journal Atmos. Chem. Phys.
Published: 24 November 2016

previous versions, the Noah LSM was overestimating surface temperature over sea ice in case of snow melt over ice, particularly in late spring and summer as found by Marelle et al (2016). This can interfere with the air mass exchange with mid-latitudes, and increased vertical mixing from lower stability.

The other LSM model used in this study is the NoahMP scheme (Yang et al., 2011). NoahMP contains a multi-layer snow pack with liquid water storage and melt/refreeze capability and a snow-interception model describing loading/unloading, melting/refreezing, and sublimation of the canopy-intercepted snow (Niu, et al., 2011). It considers equations for the snow albedo, snow temperature, density, total water content and content of liquid water which help to improve simulations of the diurnal variations of the snow skin temperature, which is critical for computing available energy for melting (Chen et al., 2014; Niu, et al., 2011). Studies comparing Noah and NoahMP (e.g. Miguez-Macho and Fan, 2012) have shown that NoahMP tends to show larger daytime biases in the diurnal cycle of the 2-m temperature and dew point during wet months compared to dry moths. The same studies also indicated that monthly absorbed SW radiation and sensible heat shows that less solar radiation is absorbed in Noah then in NoahMP resulting in a colder surface and a lower (or negative) sensible heat flux.

2.1.2 Initial and lateral boundary conditions

High quality data are needed in order to minimize the uncertainties introduced by the initialization of the model and the provision of the lateral boundary conditions required during run-time. Reanalysis datasets used for initialization and to create lateral boundary conditions are created from a combination of both observed (assimilated) variables (e.g., temperature,) obtained from different sources (e.g. ground-based observations and radiosondes), and derived fields (e.g., precipitation and cloudiness). These variables are assimilated into a global, gridded, and temporally homogeneous dataset making the best possible use of a large number of observations (Dee et al., 2014).

In this work two reanalysis datasets are used for the model initialization and to recreate the lateral boundary conditions: the ERA-Interim reanalysis (Dee et al., 2011) produced by the European Centre for Medium-Range Weather Forecasts (ECMWF) and the Arctic System Reanalysis (ASR) (Bromwich et al., 2010). ERA-Interim is a global reanalysis of recorded climate observations over the last 30 years with an improved atmospheric model and assimilation system and replaces its predecessor ERA-40 using four-dimensional variational data assimilation (4D-Var). ERA-interim is available as a gridded data set at approximately 0.7° spatial resolution and 37 atmospheric pressure levels (Dee et al., 2011). Some studies have shown that ERA-Interim agree well with observations of sea level pressure, near-surface air temperature, surface shortwave and longwave radiative fluxes, precipitation, and wind speed when compared against other reanalysis datasets (refer to Lindsay et al., 2014). However, global reanalyses like ERA-interim have many known problems at high latitudes for different reasons including the scarcity of observational data at these remote areas.

On the other hand, the ASR, developed by the Polar Meteorology Group (PMG) of the Byrd Polar Research Center (BPRC) at the Ohio State University in collaboration with several other institutions is a reanalysis recently developed which implements parameterizations optimized for the Arctic. It consists of a high-resolution version of the Polar Weather Forecast Model (PWRF) and the WRF-VAR and High Resolution Land Data Assimilation (HRLDAS) (Bromwich et al., 2016). PWRF is available through the NCAR Research Data Archive (NCAR, 2015). In this study, we use the ASRv1 30-km consisting of a gridded dataset at a spatial resolution of 30 km and with 29 pressure levels. The data set consists of 27 surface and 10 upper air (measurements in the part of the atmosphere above Earth's surface) variables and 3 soil variables. Differences in the reanalyses used to create the forcing data for our WRF simulations might have a significant impact on the modeled meteorological fields. A comparative analysis of both reanalyses is given in the following section whereas the results from the WRF model simulations to assess the differences resulting from the initial and boundary conditions are presented in section 3.

Comparison between ERA-interim and ASR reanalysis

The capability of both reanalysis to represent the Arctic atmosphere has been recently compared and documented (e.g. Wesslén et al., 2014; Bromwich et al; 2016). For example, Wesslén et al. (2014) found that while ERA-Interim has a systematic warm bias in the lowest troposphere, ASR has on average a cold bias of about the same magnitude. These authors also found that improvements in the modeled cloud properties, radiation budget, and surface temperature in ASR were not significant in spite of its more sophisticated parameterizations of cloud microphysics. In a more comprehensive assessment of the differences between both reanalysis, Bromwich, et al (2016) found that in higher latitudes throughout Europe, Siberia and North America, the ASR biases are small and cool, whereas ERA-Interim shows warm biases across much of the domain, particularly across Siberia, Alaska and western North America. The authors argue that this trend is probably related to the complex topography in these regions. This is because accurate simulation of near-surface winds over complex terrain is particularly challenging due to highly variable small scales resulting in winds that are not always well represented on a coarse model grid.

In our study, we evaluate the differences in four important variables (2m temperature and 10m wind speed, sea ice fraction and sea level pressure) between both reanalyses over our studied domain. Fig. 1 shows the differences between both reanalyses for the five-year average for the summer (JAS) and winter (FMA). Biases in the near-surface variables are generally smaller and temperatures are generally colder in the ASR than in ERA-interim. This agrees with the typical biases described in Bromwich et al. (2016) who also found a good agreement in the near-surface moisture and wind fields when compared against observational data. ERA-Interim tends to show larger values than ASR of 10m wind speed over the high Artic Ocean characterized by sea-ice covering, whereas 10m wind speed tends to be underestimated over continental area, specifically over the east coast of Greenland (Fig. 1). This is consistent with the findings from Moore et al (2013). In their study they found that ERA-Interim has surface wind speeds over the Scoresby Sund region of east Greenland that are too low and not entirely consistent with observations of topographically forced drainage flow in this region. However, when compared against observations in our study, both reanalyses tend to slightly underestimate wind speeds (see section 3.2). Previous model studies have demonstrated that ERA-Interim leads to overly strong turbulent mixing (i.e. Jung et al., 2010), which leads to weak inversions, warmer temperatures near the surface and stronger horizontal wind. As for sea-ice (fourth row in Fig. 1), both datasets are very consistent for both FMA and JAS seasons. However, in the ERA-Interim reanalysis, several locations near the Russian coastline and in some water bodies in North Europe have a larger sea-ice fractions (~0.3) compared to the ASR, especially during the FMA period. This can be explained by the fact that ASR uses MODIS sea ice data. Also the sea ice thickness and snow cover on sea ice vary in ASR whereas these values are fixed in ERA-Interim. Not included in our analyses are the differences at all atmospheric levels; Bromwich et al (2016) found that temperatures are similar with annual mean biases within ±0.2°C at nearly all levels from both reanalyses. However, Jakobson et al. (2012)

found that during spring and summer over the Arctic Ocean most reanalyses (including ERA-Interim) have large errors in the vertical profiles of air temperature as well as specific and relative humidity.

2.1.3 The WRF-Chem model

We also conduct selected case studies with the Advanced Research WRF (ARW) including chemistry and aerosols (WRF-Chem) version 3.7.1. WRF-Chem is capable of calculating chemical processes online including the feedback of radiatively active trace gases and aerosols on atmospheric dynamics. Additional processes simulated by WRF-Chem include emissions, transport of chemical species and aerosols, chemical transformation of species, aerosol physics (e.g., nucleation, condensation and coagulation), interaction of particles with radiation (photolysis and heating rates), aerosol-cloud interactions (cloud condensation nuclei), and wet and dry deposition to the surface (Grell et al., 2005; Peckhman et al., 2011). In earlier versions of the model, the Noah LSM was overestimating surface temperatures over sea ice in case of snow melt over ice leading to possibly increased exchange with the mid-latitudes and increased vertical mixing from lower stability. This may be one of the reasons why concentrations of BC have been simulated poorly in versions of WRF-Chem prior to v3.7 such as the results published in Eckhardt et al (2015).

For the case studies with the WRF-Chem model, we use the same physical parameterizations summarized in Table 1 plus the input data and chemistry/aerosols configuration (Table 2) applied in previous modeling studies over the Arctic (e.g., Grell, et al., 2011; Marelle et al., 2016). For the simulation of aerosol processes, we use the MADE/SORGAM scheme (Modal Aerosol Dynamics model for Europe, Ackermann et al., 1998 / Secondary Organic Aerosol Model, Schell et al., 2001). The MADE/SORGAM scheme simulates the aerosol size distribution using a modal approach with three overlapping log-normal modes. Within each mode, all particles are assumed to have the same chemical composition (internal mixture). This is important factor because the interaction of aerosols with chemistry or atmospheric processes depends on their size and the chemical composition (Baklanov et al., 2014). The aerosol processes are coupled to the clouds and radiation, including photolysis, and gas-phase chemistry. Aerosol and chemistry variables are initialized from the global chemistry model MOZART. More details on WRF-Chem can be found in Peckham et al. (2011), Grell et al. (2005) and Fast et al. (2006).

Emissions

Emission data are an important model input as their quality determines to a great extent the results when modeling air pollutants. In this study, anthropogenic emissions are obtained from the EDGAR HTAP v2.2 inventory (EDGAR: Emission Database for Global Atmospheric Research), created in joint collaboration between the European Commission, and the Task Force on Hemispheric Transport of Air Pollution (TF HTAP). EDGAR HTAP v2.2 reports monthly anthropogenic emissions of greenhouse gases (e.g. CO_2, CH_4 and N_2O), precursor gases (e.g. CO, NO_x and SO_2) and aerosols (PM10) per source category at country level on 0.1° × 0.1° grid maps from the energy, industry, transport and residential sectors and annual emissions from shipping and aviation. Emission data from small agricultural fires are not included in v2.2 and were taken from the previous version EDGAR HTAP v1.0. Information about methodology and emission factors used for the EDGAR emission calculations is well documented in Janssens-

Maenhout et al. (2015). Biological emissions are included applying MEGAN (Model of Emissions of Gases and Aerosols from Nature), which calculates biogenic emissions online based on simulated temperature, leaf area index and land use data (Guenther et al., 2006). For biomass burning emissions, we used the Fire Inventory (FINN) version 1 also developed by NCAR. FINN is based on daily satellite observations of fires and land cover, combined with emission factors and estimated fuel loadings (Wiedinmyer et al., 2011).

2.1.4 Model domain and simulations

The WRF model setup used in this study consist of a single domain covering the Eurasian Artic region at a horizontal resolution of 15 km over an area of approximately 4000 x 3800 km (centered at 70°N and 40°W), which includes large parts of northern Europe and North-west Russia (Fig. 2). The atmosphere is vertically resolved in 30 full σ-levels with 15 model levels below $\sigma = 0.9$. The lowest model level in this configuration is centered at 10 meters, whereas the model top-level pressure is set at 100 hPa. The reason for such high vertical resolution in the lowermost troposphere is based on the premise that vertical mixing and turbulent fluxes which are key processes in the PBL may be affected by the total number of vertical levels and in particular by the number of vertical levels close to the surface. For example, recent studies suggest a strong sensitivity to the modeled 10-m wind speed on the model's vertical resolution (i.e. Chou, 2011; Kleczek et al., 2014).

Simulations with the atmosphere -only model WRF were performed over 5 cold (February, March and April) and 5 warm (July, August and September) seasons from the year 2008 to 2012 coinciding with the maximum and minimum sea ice extent in the region. These periods are also characterized with the minimum (warm period) and maximum (cold period) observed concentrations of BC over the Arctic above 66°N (Stohl et al., 2013). Four different sensitivity analyses were performed and named according to the configuration chosen, as described later and also shown in Table 1b. The sensitivity analyses are aiming at quantifying the impact of the different LSMs and reanalyses used for the creation of the initial and lateral boundary conditions on model biases compared with surface measurements as well as observed vertical profiles of meteorological variables from stations in the Eurasian Arctic.

Finally, we analyze a suite of selected cases using WRF-Chem (summarized in Table 2) to assess how the model simulates BC transport into the domain. This is important to estimate the uncertainty of the climate impact of BC transported into the Arctic when assessing different emission scenarios. These case studies with WRF-Chem include 1-month simulations for April 2008, July 2008, April 2009 and July 2010. The case studies were selected based on the availability of observational data used for comparison with the model results. The year 2008 coincides with the Polar International Year in which several ground and aircraft campaigns took place. Also, some authors have described exceptionally high forest and agricultural fire activity in Russia, Kazahkstan and Southeast Asia in April 2008 (Warneke et al., 2009; Fisher et al., 2010). We therefore also include April 2009 as an additional case study for comparison with the previous year. July 2010 was an exceptionally hot summer (the hottest summer since the year 1500) impacting in particular Western Russia and resulting in a historical heat wave which triggered 500 wildfires around Moscow (Barriopedro et al., 2011). Such wildfires could be important emission sources of BC transported into the Arctic. Previous studies have demonstrated that fires in Eastern Europe and Russia can lead to substantial increases in the atmospheric loading of pollutants at several surface sites in the European Arctic (Stohl et al., 2007) which we aim to confirm with the simulations carried out in the present study.

2.2 Observational data for model evaluation

2.2.1 *Meteorological data*

Surface meteorology in the model is evaluated against observations from 24 weather stations in North Europe and Russia spread throughout the model domain with data available for the studied period and acquired from the Met Office Integrated Data Archive System (MIDAS) (Fig. 2). The southernmost station is "*Leningrad*" at 59.95°N, located in the city of Saint Petersburg, whereas the northernmost station is "*Krenkelja*" at 80.64°N in the Franz Josef Land located between the Arctic Ocean, and the Barents and Kara Seas. The MIDAS dataset comprises daily and hourly weather observations including hourly wind parameters, maximum and minimum air temperature, soil temperature, sunshine duration and radiation fluxes as well as daily, hourly and sub-hourly precipitation measurements, some climatological data and marine observations. The reporting frequency varies among the different stations. At best the data are hourly although some stations report only at 0600, 1200 and 1800 local time (*Met Office*, 2012). In this study we evaluate the root mean square error (RMS) of both reanalysis used for creating the initial and boundary conditions (ERA-Interim and ASR) together with the time series from the different WRF sensitivity experiments for temperature, wind speed, water vapor mixing ratio and snow depth. Bias and RMS are calculated from the comparison between model simulations and surface observations over the five year period 2008-2012. In order to facilitate the analysis, the 24 observational stations where divided into two groups: 1) stations located inside the Arctic Circle (here defined as 66°N 34') and 2) those stations located below the Arctic Circle (Table 3).

We also use observed vertical profiles of temperature, wind speed and relative humidity from the enhanced version of the Integrated Global Radiosonde Archive (IGRA) (http://www1.ncdc.noaa.gov/pub/data/igra/) to examine both the variability during the five year period and to assess the model performance and the reanalyses in reproducing the vertical structure of these variables. The IGRA dataset consists of quality-controlled radiosonde and pilot balloon profiles, freely available at more than 1500 globally distributed stations covering varying time periods, many with observations extending from the 1960s to the present (Durre et al., 2006). Upper air data are usually measured by twice daily by radiosonde soundings, taken at 00 and 12Z (Greenwich time). As can be seen in Fig. 2, there are only very few long-term surface measurements in the high Arctic, especially in the North Russian Arctic. Nevertheless, the available stations are helpful to provide a snapshot of the vertical structure of the Arctic atmosphere and to test model performance.

2.2.2 *Aerosol observations*

Routine measurements to monitor atmospheric chemistry components in the Eurasian Arctic are very scarce. The limited availability of long-term measurements results in a high uncertainty of the estimated climate impacts of aerosols in the Arctic. In order to help filling these gaps and to improve our understanding of Arctic pollution, intensive field campaigns including surface and aircraft observations have been conducted in recent years. In addition, surface based sun photometer instruments like the AERosol NETwork (AERONET) provide information on aerosol loading and aerosol optical depth as well as other physical properties. AERONET is an optical ground-based aerosol-monitoring network and data archive consisting of identical automatic sun-sky scanning spectral photometers operated by national agencies and universities (Holben et al., 1998). There are, however, only very few long-term observations from the AERONET network available close to the Arctic Circle. Seven AERONET stations were selected in this study (Fig. 2) for an initial evaluation of the model performance. In addition, available observations of Equivalent Black Carbon and measurements of the size integrated aerosol particle number concentration (PNC) measured by a Condensation Particle Counter (CPC) from the monitoring EBAS database (EBAS, 2013) operated by the Norwegian Institute for Air Research (NILU) are used for comparison with our model simulations. All data are available from the EBAS database (http://ebas.nilu.no/).

3 Results

3.1 Meteorological analyses

3.1.1 Large scale atmospheric circulation

The pattern of the large scale circulation during the five year period is shown for two sensitivity experiments (*noahmp_asr* and *noahmp_ecmwf*) in Fig. 3 for winter (February, March and April) and in Fig. 4 for summer (July, August, September) averaged over five years (2008-2012). The position of the polar dome in our domain is also calculated given its importance as proxy for studying the transport of pollutants and its implications (Stohl, 2006). Here we define the polar dome following Jiao and Flanner (2016) by calculating the maximum latitudinal gradient of the 500 hPa geopotential height. The reasoning for this approximation is that where the latitudinal geopotential height gradient is largest, the zonal component of the geostrophic wind is likely to be strongest, and this narrow band of strong geostrophic wind plays an important role for tracer transport in the middle troposphere (we refer to Jiao and Flanner (2016) for further details). Jiao and Flanner (2016) also suggest that the northward expansion of the polar dome correlates with warming in some regions in Alaska and Chukchi Sea. In this work, the calculated isopleth defining the polar dome (gray line in Figs. 3 and 4) extends to middle-latitude regions in the winter months (FMA) when the jet wind speed reaches its maxima as a result of the stronger temperature gradient between low- and high-latitude regions.

In general, the differences between both reanalyses used to drive the model (see section 2.1.2) are also noticeable in the model outputs. The persistence of the Icelandic Low (the low-pressure center located usually between Iceland and southern Greenland) is visible in both WRF experiments. The low pressure area generally has an elliptic shape and is located near 90°N and 30-50°W, also described by Sahsamanoglou (1990). The low pressure weakens and splits into two centers in summer, one near Davis Strait and the other west of Iceland during the FMA period in the experiments using the ASR data (left column), whereas this pattern is highly variable in the experiments using ERA-Interim reanalysis for initialization and as lateral boundary conditions (right column). For the winter period FMA (Fig. 3), there is a particularly strong average low pressure region in the year 2011, also reflected in high wind speeds at 850hPa (~17 m/s) over a large portion of the North Atlantic Ocean over the model domain. In the model experiments using ASR data, wind speeds tend to be higher than in the experiments using ERA-Interim data during all years analyzed. High wind speeds are also simulated over central Russia in both experiments during 2008. As for the summer period (JAS) shown in Fig. 4, the low pressure region is less well defined. Notice that in summer 2010, cyclonic activity tends to be high with a significant increase in wind speed, particularly over the Kara Sea, with 10m wind speeds as high as 11m/s

Atmos. Chem. Phys. Discuss., doi:10.5194/acp-2016-942, 2016
Manuscript under review for journal Atmos. Chem. Phys.
Published: 24 November 2016

over a vast area of North-West Russia. The year 2010 was characterized by a strong heat wave that affected a large part of North-West Russia. This event was linked to a combination of a very strong low pressure system near Iceland and a less intense than usual low pressure system located near the North Pole (Trenberth and Fasullo, 2012). This is also reflected in the position of the Polar Dome which is displaced further south in winter time, particularly in the *noahmp_ecmwf* experiment (Fig. 3).

It has been noted in previous research that this anomalously cold winter in 2009/2010 was followed by an abrupt shift to a warmer-than-normal early growing season (the Russian heat wave took place in summer 2010) which was consistent with a persistently negative phase of the North Atlantic oscillation (NAO) (Wright et al, 2014). This cold winter was characterized by unusually cold and snowy conditions over China and eastern Asia, the eastern United States and Europe that lasted until February 2010. In contrast, other regions such as west Greenland and the Bering Strait experienced anomalous warm temperatures (Seager et al., 2010).

3.1.2 Surface meteorology

Fig. 5 shows the spatial distribution of the planetary boundary layer height (PBLH) calculated by the model for all sensitivity experiments for the winter (Fig. 5a) and for summer months (Fig. 5b). The PBLH from the model is calculated by the PBL scheme and is based on the bulk Richardson number method. A detailed description of the methods used to calculate the PBLH in the scheme can be found in Hong (2010). The Arctic atmosphere is stably stratified most of the year with the lowest kilometer of the atmospheric column north of 70°N almost permanently stably stratified. This is more pronounced during winter than in summer as seen, for instance, in the representation of the planetary boundary layer height in Fig. 5. In winter the average modeled PBLH oscillates around 1000 m over the ocean in the North Atlantic sector between the Svalbard Archipelago and the Nordic countries (Fig. 5a). However, there are significant differences in the PBLH close to 90°N, where the model experiments using the ASR data simulate a deeper PBLH (~250 m) compared to those obtained using the ERA-Interim reanalysis (~150 m). In summer (Fig. 5b), the PBLH is deeper over the continents due to the large insolation during this period resulting in convective mixing. The PBLH over the Arctic Ocean continues to be lower than in winter due to the increasing solar radiation over high latitudes. In the experiments using the NoahMP scheme, the PBLH is generally deeper over the continent than in those using the Noah LSM scheme in both seasons. Particularly over the Nordic countries and Russia in winter, the values are between the 400-450 m compared with a shallower PBLH obtained with the Noah scheme (~200-350 m) independent of the reanalysis used. The differences in PBLH between the two LSMs occurs at the time of day when the PBL becomes a shallow layer after sunset as also reported by previous studies (e.g. Pino et al., 2006; Milovac et al., 2016). Misenis and Zhang (2010) suggest that NoahMP simulates a later daily collapse of the PBL of at least 30 min which might also be related to wind shear at the top and bottom of the PBL. This may have important implications on other meteorological variables as described by Misenis and Zhang (2010).

The differences in the main meteorological variables analyzed here, i.e. sea level pressure (SLP), 2m temperature and 10m wind speed are summarized for the individual sensitivity experiments in Table 4. All sensitivity analyses tend to show stronger cold biases in 2m temperature than the reanalyses used to create the initial and lateral boundary conditions. These cold biases over the region have been also found by other authors (i.e. Déqué et al., 2007, Katragkou, et al 2015). Katragkou et al (2015) suggest that coldest mean temperature bias in northern Europe is related to an underestimation of SW radiation at the surface and an overestimation of cloud cover. This is particularly seen in WRF model configurations using the Grell convective scheme (also used in our experiments). The spatial distributions (Fig. 6) of the modeled 2m temperature, 10m wind speed and SLP match those estimated from the observational data at the 24 stations dispersed throughout the domain (colored circles in Fig. 6) reasonably well for the winter months (left column) and summer months (right column).

In order to investigate the temporal agreement between the simulated and observed meteorological variables from the 24 stations used to validate the model simulations, Taylor plots are used. These diagrams provide a statistical summary of how well observed and simulated 3-month time series match each other in terms of their temporal correlation (R) and normalized standard deviation (NSD) (Taylor, 2001). In the Taylor diagram R and NSD are given in this polar projection by the angular and the radial coordinate, respectively (Fig. 7). The reference point (observations) is located at x=1, y=0. The linear distance between a model and the reference point is proportional to the RMS error making it easy to identify the stations for which the model experiments perform well. The correlation in 2m temperature ranges between 0.45 and 0.85 depending on the model simulation and the station. In general, there is a large spread among the different model experiments and measurement stations with no model configuration being clearly superior at all measurement stations. Also the temporal standard deviation of the model experiments varies widely among the different experiments and for the different stations. This large spread is even more pronounced for the time series of 10m wind speed. For 10m wind speed, the NSD from the model results is typically much larger than 1 with maximum values of up to 4. This overestimation in 10m wind speed in the model experiments can also be seen in Fig. 6, with the overestimation being particularly pronounced over the continent.

Given the sparsity of available long-term surface measurements, it is difficult to assess which model experiment performed better compared to observations using only Taylor diagrams. We therefore also calculated biases and RMS (shown in Table 4) in which we separate the stations in two groups, those below and those above the 60°N, and also include both reanalyses (ERA-Interim and ASR) in the comparison with observations. In general for the studied domain both reanalyses are slightly warmer in the winter months (FMA) with ERA being 0.40°C and ASR 0.18°C warmer at stations above the 66°N and slightly negative biases in stations outside the polar circle with -0.12°C and -0.28°C, respectively. A slightly negative bias in the summer months (JAS) in all the model experiments is persistent for all the stations. In Bromwich et al (2016), the authors indicate that ASR may be little cold over sea ice. Our model experiments also show a similar negative bias tendency as the ASR reanalysis for all variables. For 10m wind speed, the ERA-Interim data show slightly positive biases of less than 1 m/s at all the stations in the two seasons. ASR biases are quite small but tend to be negative. With regard to sea level pressure, both reanalyses generally show slightly negative biases in all seasons ranging from -0.03 to -0.59 hPa.

3.1.3 Atmospheric vertical structure

Vertical gradients in potential temperature and wind speed are good diagnostics to estimate the transport pathway of emissions as shown for example in Aliabadi et al. (2015). Fig. 8 shows the radiosonde profiles at three stations around our domain for temperature, wind speed and relative humidity at 12UTC (the most data are available at this time of the

Atmos. Chem. Phys. Discuss., doi:10.5194/acp-2016-942, 2016
Manuscript under review for journal Atmos. Chem. Phys.
Published: 24 November 2016

day) averaged of the winter months (February, March and April) for the five years of study. The overall performance statistics for these meteorological variables is also summarized in Table 5. Radiosonde observations of the vertical structure of temperature and wind speed typically show stable profiles with a temperature inversion caused by the lack of surface heating by the sun. Temperature inversions inhibit convection so emissions are not lifted to higher altitudes and pollutants from the surface can become trapped close to the ground. The comparison of the vertical temperature profiles shows generally good agreement of the model experiments with observations. However for some stations (i.e Ostrov Dikson) the modeled profiles when using simple Noah scheme show closer proximity with observations than when using Noah-MP. The overestimation of the vertical temperature may be caused by a possible overestimation of the turbulent sensible heat flux towards the surface causing premature warming along the vertical column. This may not be the case of stations located in urban areas such as Leningrad station which shows more consistency in modeled profiles compared to the observations. Wind speeds tend to be overestimated in the model. These positive biases in wind speed have been reported in other locations with complex terrain and can introduce systematic errors to the simulations (i.e. Jiménez and Dudhia, 2012; Santos-Alamillos, et al 2013). For example, Jiménez and Dudhia (2012) reported a positive bias in wind speed simulated with WRF over plains and valleys whereas negative biases may be present over hills and mountains. The unresolved topographic features can produce additional drag, which is not parameterized in the WRF, in addition to the drag generated by vegetation. The magnitude of this bias is related to the differences between the actual and the elevation of the stations in WRF (Santos-Alamillos, et al 2013). Again, there is no particular model configuration that clearly outperforms the other WRF sensitivity simulations. The radiosonde observations are close to the lateral boundaries of the model domain. As measurements are very sparse in this region, also the reanalysis data used as lateral boundary conditions are subject to large uncertainties translating directly into the model results and can possibly overcompensate the effect of other model configuration options such as the choice of LSM.

For the model simulations with WRF-Chem, we therefore use the configuration that includes the most processes relevant to modeling BC transport into the Arctic, the configuration using the ASR reanalysis and the NoahMP LSM scheme. Even though the ASR/NoahMP configuration shows slightly smaller biases in simulated wind speed than the other configurations, the evaluation of the simulated meteorology did not show a clearly superior configuration for all variables analyzed. We regard this slightly small bias in wind speed as an advantage because of the importance to simulated transport pathways of pollutants.

3.2 Case studies using WRF-Chem in the Eurasian Arctic

Atmospheric chemistry models have struggled for a long time to capture the observed distribution of aerosols in the Arctic (Shindell et al., 2008; Koch et al., 2009, Eckard, et al 2015). The concentrations of BC during the Arctic Haze season (winter to early spring) are typically underestimated whereas summer concentrations are sometimes overestimated, in some cases by more than an order of magnitude (Shindell et al., 2008). In this study, several cases covering the periods of maximum and minimum BC over this region coinciding with the availability of measurement data for the model evaluation were selected within the five years used to evaluate the meteorology. The aim is to assess the performance of the model in calculating concentrations of specifically BC over our model domain and to analyse possible linkages with the modeled atmospheric circulation during this period.

3.2.1 Aerosol Optical Depth

We first assess the model AOD at 550 nm against observations from AERONET sun-photometers for the four case studies using WRF-Chem to investigate the model's performance in representing spring/summer high/low aerosol loadings. The aerosol loadings are expected to include a significant contribution from BC, especially at sites close to urban or industrialized centers. Fig. 9 shows the modeled spatial distribution of AOD for the four cases April and July 2008 and April 2009 and July 2010. High aerosol loadings over northern Europe and western Russia are modeled with monthly mean values typically in the range of 0.1-0.2. Maximum AOD values are modeled in April 2008 with values exceeding 0.35 particularly over parts of western Russia. Several authors have reported that the Arctic AOD is mostly dominated by sulfate in spring and organic carbon (from fires) in summer (Breider et al., 2014). Our model results agree reasonably well with AOD observations in July 2008 at most of the selected stations (colored circles in Fig. 9a), but overestimates AOD by about 0.1 in April 2008 and underestimates AOD by up to 0.1 in July 2010. Besides the lateral boundary conditions for aerosols, also the emissions play a crucial role in the modeled aerosol loadings resulting in differences between modeled and observed AOD. The modeled AOD also strongly depends on the relative humidity as particles taking up water are more efficient in scattering light. Particularly in the range of high relative humidities, even small errors in the modeled relative humidity can result in significant differences in the modeled AOD.

Also shown in Fig. 9b is a Taylor diagram comparing the observed time series of AOD at the AERONET stations with the model results. The temporal correlation between model results and observations depends strongly on the month simulated and ranges between 0.2 for April 2008 and 0.75 for July 2010. In most cases, the model overestimates the temporal standard deviation of AOD which is related to a general overestimation of AOD at these stations, The only exception is for July 2010, where the model tends to underestimate AOD values, as also observed in the spatial distribution in Fig 9a. This fact can be highly dependent on the fire emission data which causes the model to under predict amounts of burned areas, particularly for those stations located in west Russia which results in model underestimating non-dust AOD. This problem could potentially be solved by testing another more advanced biomass inventory of monthly burned area (e.g. the latest Global Fire Emissions Database, Version 4 (GFEDv4.1) biomass inventory, also described in Randerson et al 2015).

3.2.2 Black Carbon

The highest modeled BC loadings in Russia typically correspond to the large urban areas (i.e. Moscow and St. Petersburg) and less to locations close to the Barents Sea where oil exploration and exploitation sites are located (Fig. 10). Koch et al. (2009) found that many models underestimate BC at northern latitudes because of an overestimation of BC scavenging (especially wet deposition) and vertical mixing during poleward transport. Observed high concentrations of BC in April are characteristic for the high aerosol loadings typically found in late winter and early spring, which is qualitatively reproduced by the model (Fig. 10). During this period of the year, conditions are generally favorable for the transport of air pollutants into the Arctic forming the Arctic haze. For example, in April 2009 the atmosphere over the European and North American Arctic was often characterized by hazy conditions with transport of air pollutants mainly from Eurasia (Stone et al., 2010). In Fig. 10 we show how concentrations for BC vary in the different months simulated. The high BC concentrations observed in Russia are currently not captured by model suggesting an underestimation of BC emissions in Russia in current emission inventories (Stohl et al., 2013; Eckardt et al., 2015). Warneke et al. (2009) reported a substantial contribution from Russian forest fires and central Asian agricultural burning to atmospheric pollution over the Arctic.

Long-term measurements of BC in the Arctic are very sparse, but data from measurements performed at Zeppelin station (475 m a.s.l), near Ny-Ålesund are available for comparison with the model results for April and July 2008. The modeled BC is averaged over the 3 × 3 nearest grid points surrounding the measurement station and calculated from the concentrations in the lowest two model layers, centered around about 30 m above the ground.

The Zeppelin station observations (Fig. 11a) show 3-5 times higher BC concentrations in April compared to July. This difference is qualitatively reproduced by the model. The vertical distribution of BC (Fig. 11b) shows that concentrations larger than 20 ng/kg are simulated in April up to 200 hPa, whereas there is little to no BC simulated above 500 hPa in July. This is consistent with the idea that BC from source regions outside the Arctic is transported most efficiently into the Arctic in spring, whereas the is little to no long-range transport in summer. The model results suggest that a considerable amount of BC aerosols originating from Europe and East Asia have been lifted into higher altitudes (middle and upper troposphere) and transported over the northern oceans (Fig. 11b). BC aerosols in these high-latitude areas are relatively long-lived due to lower wet scavenging compared to the mid- and low latitudes. The WRF-Chem simulations performed in this study show a mean BC concentration in spring of 0.1 ± 0.1 µg/kg north of 60°N, which is consistent with model simulations done by other authors (Breider et al., 2014 with 0.12 ± 0.05 µg/kg).

Fig. 11c shows the probability density functions (PDFs) calculated from the observed and modeled BC concentrations at Zeppelin station. The model clearly overestimates the cases with very low BC concentrations in April and in July and does not reproduce the highest observed BC concentrations. In April, the shape of the PDF for values above 0.02 $\mu g/m^3$ is qualitatively reproduced by the model even though the absolute values are underestimated by a factor of 5. This is, however, not the case in July where the observations and modeled PDF are relatively flat for BC concentrations no larger than 0.015 $\mu g/m^3$ for the model This might indicate a missing close-by BC source in the model that could be the reason for the observed larger occurrences of BC up to 0.045 $\mu g/m^3$compared to those in the model.

Measuring the atmospheric concentration of BC is subject to higher uncertainties than, for example, sulfate measurements (e.g. Sharma et al., 2004). Because of this, among other reasons, only few atmospheric BC measurements in the Arctic are currently available. Cavalli et al. (2010) pointed out that the BC atmospheric concentration can vary by a factor 5 depending on the observation protocol; on the model's part, both, errors in emissions and in the deposition parameterizations can strongly affect the results. In our simulation, we used monthly emissions from fossil fuel combustion and daily emissions from large forest fires. This relatively coarse time resolution of the emissions certainly contributes to our simulation biases. In the real world, emissions can be quite variable, with substantial implications for the BC concentration observed throughout the atmosphere. Other complex physical processes are coarsely represented in our model and are expected to also contribute to our model biases.

4 Summary, Conclusions and Outlook

In this work, we assessed first the role of the choice of the land surface model (Noah and NoahMP), which is part of the physical parameterization suite of WRF together with the choice of reanalyses used for initialization and to create lateral boundary conditions. Biases in the modeled meteorology (e.g. wind speed and direction, boundary layer height) are expected to influence the modeled BC concentrations. As the modeled meteorology strongly depends on the model configuration used, the impact of the choice of data used for initialization and lateral boundary conditions and the choice of LSM scheme was systematically investigated in several model experiments. The results showed that no particular model configuration clearly outperforms the other model configurations when compared to available Arctic observations. Usage of the higher resolution ASR data or a more sophisticated formulation of land surface processes (NoahMP) did not systematically improve model performance in the Arctic. The results suggest that there are other factors to consider such as, for example, the accurate simulation of the Arctic sea ice decline, stratosphere-troposphere interactions, atmosphere-ocean interaction, and boundary layer processes. Improvements of surface albedo, for example, could be achieved by taking more advantage of continuous and reliable satellite and ground-based data for calibration and comparison purposes. This study can therefore also be seen as a starting point for further, systematic sensitivity studies to assess the impact of individual factors such as meteorological model performance, model resolution, boundary conditions, soil characteristics, and the various parameterizations within the physical schemes on the model results for air pollutants in the Arctic.

This study is a contribution to ongoing work aiming to evaluate the capability of WRF-Chem to simulate BC around the Eurasian Arctic. While the modeled BC concentrations are qualitatively consistent with observations in terms of spatial distribution and time series, the modeled concentrations of BC are too low in the Russian Arctic as noted by (Eckardt *et al.,* 2015). Several factors are likely to influence the modeled BC concentration besides biases in modeled meteorology. For example, Kuik et al. (2015) and Eckard (2015) found that underestimations in modeled BC concentration in WRF-Chem are also related to the low quality of the emissions data. This has important implications for the projected changes in Arctic climate when model natural dynamics are interacting with anthropogenic emissions. Reliable emission inventories with a high temporal and spatial resolution are critical to improve the modeling of aerosols and air chemistry. Especially for this region, model simulations are an important tool to assess the contributions of individual source categories to the total BC concentrations (such as energy or industrial origin). Also, for deepening the analysis of the different impacts of anthropogenic BC it is crucial to have good observational data, e.g. for BC and particulate matter, vertical profiles of temperature and humidity. Other problems leading to systematic errors include those already found in the model. For example, Marelle, et al. (2016) found that a bug in older versions of the Noah LSM scheme that has been fixed in the current version used for this study (WRF3.7) in combination with an underestimation lack of aerosol wet removal by subgrid-scale clouds, may be one of the main factors contributing to the simulated low BC concentrations over areas dominated by an sea-ice/ atmosphere interface.

5 Data availability

The two external model data sets used in this work, ERA-Interim is available from http://apps.ecmwf.int/ (Dee et al., 2011) and Arctic System Reanalysis (ASR) available from http://rda.ucar.edu/ (Bromwich et al., 2016). The Met Office Integrated Data Archive System (MIDAS) is available at the British Atmospheric Data Centre, http://catalogue.ceda.ac.uk/. The radiosonde data from the Integrated Global Radiosonde Archive (IGRA) are available at ftp.ncdc.noaa.gov/pub/data/igra/ (Durre, et al 2006).

6 Acknowledgements

All model simulations used in this study were performed at at the high performance cluster computer of the German Climate Computing Center (DKRZ). For data processing and figures we used the open-source software NCAR Command Language (NCL) also available at https://www.ncl.ucar.edu/.

7 References

Ackermann, I.J., Hass, H., Memmesheimer, M., Ebel, A., Binkowski, F.S. and Shankar, U.: Modal aerosol dynamics model for Europe: Development and first applications, Atmospheric environment, 32, No.17, 2981-2999, 1998

Aliabadi, A. A., Staebler, R. M., de Grandpré, J., Zadra, A., and Vaillancourt, P. A.: Comparison of estimated atmospheric boundary layer mixing height in the Arctic and Southern Great plains under statically stable conditions: experimental and numerical aspects, Atmos-Ocean., doi:10.1080/07055900, 2016.

Anderson, P. S., and Neff W.D.: Boundary layer physics over snow and ice, Atmos. Chem. Phys., 8, 3563-3582, doi:10.5194/acp-8-3563-2008, 2008.

Baklanov, A., Schlünzen, K., Suppan, P., Baldasano, J., Brunner, D., Aksoyoglu, S., Carmichael, G., Douros, J., Flemming, J., Forkel, R., Galmarini, S., Gauss, M., Grell, G., Hirtl, M., Joffre, S., Jorba, O., Kaas, E., Kaasik, M., Kallos, G., Kong, X., Korsholm, U., Kurganskiy, A., Kushta, J., Lohmann, U., Mahura, A., Manders-Groot, A., Maurizi, A., Moussiopoulos, N., Rao, S. T., Savage, N., Seigneur, C., Sokhi, R. S., Solazzo, E., Solomos, S., Sørensen, B., Tsegas, G., Vignati, E., Vogel, B., and Zhang, Y.: Online coupled regional meteorology chemistry models in Europe: current status and prospects, Atmos. Chem. Phys., 14, 317-398, doi:10.5194/acp-14-317-2014, 2014.

Barlage, M., Chen, F., Tewari, M., Ikeda, K., Gochis, D., Dudhia, J., Rasmussen, R., Livneh, B., Ek, M., and Mitchell, K.: Noah land surface model modifications to improve snowpack prediction in the Colorado Rocky Mountains, J. Geophys. Res., 115, D22101, doi:10.1029/2009JD013470, 2010.

Barriopedro, D., Fischer, E. M., Luterbacher, J., Trigo, R. T., and Garc´ıa-Herrera, R.: The hot summer of 2010: redrawing the temperature record map of Europe, Science, 332, 220–224, doi:10.1126/science.1201224, 2011.

Beljaars, A. C. M.: The parameterization of surface fluxes in large-scale models under free convection, Q. J. R. Meteorol. Soc.,121, 255–270, 1994.

Breider, T. J., Mickley, L. J., Jacob, D. J., Wang, Q., Fisher, J. A., Chang, R. Y. W., and Alexander, B.: Annual distributions and sources of Arctic aerosol components, aerosol optical depth, and aerosol absorption, J. Geophys. Res.-Atmos., 119, 4107–4124, 2014.

Bromwich, D.H., Kuo Y-H, Serreze M, Walsh J, Bai L-S, Barlage M, Hines, K..M. and Slater A.: Arctic system reanalysis: Call for community involvement. Eos Trans. Am. Geophys. Union 91: 13–14, 2010.

Bromwich, D. H., Wilson, A. B., Bai, L., Moore, G. W. K. and Bauer, P.: A comparison of the regional Arctic System Reanalysis and the global ERA-Interim Reanalysis for the Arctic. Q. J. R. Meteorol. Soc., 142, 644-658, doi: 10.1002/qj.2527, 2016.

Cavalli, F., Viana, M., Yttri, K.E., Genberg, J., and Putaud, J.P.: Toward a standardised thermal-optical protocol for measuring atmospheric organic and elemental carbon: the EUSAAR protocol, Atmos. Meas. Tech., 3, 79-89, doi:10.5194/amt-3-79-2010, 2010.

Chou S.H.: An example of vertical resolution impact on WRF-Var analysis, Electron J. Oper. Meteorol., 12, 1–20., 2011.

Cohen J, Screen J A, Furtado, J.C., Barlow M., Whittleston, D., Coumou, D., Francis, J., Dethloff, K., Entekhabi, D. and Overland, J.: Recent Arctic amplification and extreme mid-latitude weather Nat. Geosci. 7 627–37, 2014.

Dee, D. P., Uppala, S. M., Simmons, A. J., Berrisford, P., Poli, P., Kobayashi, S., Andrae, U., Balmaseda, M. A., Balsamo, G., Bauer, P., Bechtold, P., Beljaars, A. C. M., van de Berg, L., Bidlot, J., Bormann, N., Delsol, C., Dragani, R., Fuentes, M., Geer, A. J., Haimberger, L., Healy, S. B., Hersbach, H., Hólm, E. V., Isaksen, L., Kållberg, P., Köhler, M., Matricardi, M., McNally, A. P., Monge-Sanz, B. M., Morcrette, J.-J., Park, B.-K., Peubey, C., de Rosnay, P., Tavolato, C., Thépaut, J.-N., and Vitart, F.: The ERA-Interim reanalysis: configuration and performance of the data assimilation system, Q. J. Roy. Meteor. Soc., 137, 553–597, 2011.

Dee, D. P., M. Balmaseda, G. Balsamo, R. Engelen, A. J. Simmons, and J.-N. Thépaut: Toward a consistent reanalysis of the climate system, Bull. Amer. Meteor. Soc., 95, 1235–1248, doi: http://dx.doi.org/10.1175/BAMS-D-13-00043.1., 2014.

Déqué, M., Rowell, D. P., Lüthi, D., Giorgi, F., Christensen, J. H., Rockel, B., Jacob, D., Kjellström, E., Castro, M., and Hurk, B.: An intercomparison of regional climate simulations for Europe assessing uncertainties in model projections, Clim. Change, 81, 53–70, doi:10.1007/s10584-006-9228-x, 2007.

Denis, B., Laprise, R. and Caya, D.: Sensitivity of a regional climate model to the resolution of the lateral boundary conditions, Clim. Dyn., 20, 107–126, 2003.

Dethloff, K., Rinke, A., Lehmann, R., Christensen, J.H., Botzet, M., Machenhauer, B. : A regional climate model of the Arctic atmosphere. J Geophys Res 101:23401–23422, 1996.

Dethloff, K., Abegg, C., Rinke, A., Hebestadt, I.. And Romanov, V. F.: Sensitivity of Arctic climate simulations to different boundary-layer parameterizations in a regional climate model. Tellus A, 53: 1–26. doi:10.1034/j.1600-0870.2001.01073, 2001.

Diaconescu, E. P, Laprise, R. and Sushama, L. :The impact of lateral boundary data errors on the simulated climate of a nested regional climate model. Clim Dyn 28:333–350, 2007.

Dirmeyer, P. A.: The terrestrial segment of soil moisture–climate coupling, Geophys. Res. Lett., 38, L16702, doi:10.1029/2011GL048268, 2011.

Dudhia, J.: Numerical study of convection observed during the Winter Monsoon experiment using a mesoscale two–dimensional model, J. Atmos. Sci., 46, 3077–3107, 1989.

Duffy, P. B., Govindasamy, B., Iorio, J. P., Milovich, J., Sperber, K. R., Taylor, K. E., Wehner, M. F., Thompson, S.: High-resolution simulations of global climate, part 1: present climate, Clim. Dyn., 21, 371–390, 2003.

Durre, I., R. S. Vose, R.S. and Wuertz, D.B.,: Overview of the integrated global radiosonde archive, J. Clim., 19, 53–68, 2006.

EBAS: Observation data of atmospheric chemical composition and physical properties (http://ebas.nilu.no/) accessed 13 November 2015.

Fan, Y., G. Miguez-Macho, C. P. Weaver, R. Walko, and A. Robock: Incorporating water table dynamics in climate modeling, Part I: Water table observations and the equilibrium water table simulations. Journal of Geophysical Research-Atm, doi:10.1029/2006JD008111, 2007.

Fast, J. D., Gustafson Jr., W. I., Easter, R. C., Zaveri, R. A., Barnard, J. C., Chapman, E. G., and Grell, G. A.: Evolution of ozone, particulates, and aerosol direct forcing in an urban area using anew fully-coupled meteorology, chemistry, and aerosol model, J. Geophys. Res., 111, D21305, doi:10.1029/2005JD006721, 2006.

Grell, G. A, and Devenyi, D.: A generalized approach to parameterizing convection combining ensemble and data assimilation techniques, Geophys. Res. Lett., 29(14), doi:10.1029/2002GL015311, 2002.

Grell, G. A., Peckham, S. E., Schmitz, R., McKeen, S. A., Frost, G., Skamarock, W. C., and Eder, B.: Fully coupled "online" chemistry within the WRF model, Atmos. Environ., 39, 6957–6975, 2005.

Guenther, A., Karl, T., Harley, P., Wiedinmyer, C., Palmer, P. I., and Geron, C.: Estimates of global terrestrial isoprene emissions using MEGAN (Model of Emissions of Gases and Aerosols from Nature), Atmos. Chem. Phys., 6, 3181-3210, doi:10.5194/acp-6-3181-2006, 2006.

Handorf, D. , Jaiser, R. , Dethloff, K. , Rinke, A. and Cohen, J. : Impacts of Arctic sea-ice and continental snow-cover changes on atmospheric winter teleconnections, Geophys. Res. Lett., 42, 2367-2377, 2015.

Hines, K. M., and Bromwich, D. H.: Development and testing of Polar WRF. Part I. Greenland Ice Sheet Meteorology, Mon. Wea. Rev.,136, 2008.

Holben, B. N., T. F. Eck, I. Slutsker, D. Tanré, J. P. Buis, A. Setzer, E. Vermote, J. A. Reagan, Y. J. Kaufman, T. Nakajima, F. Lavenu, I. Jankowiak, and Smirnov, A.: AERONET - a federated instrument network and data archive for aerosol characterization, Remote Sens. Environ., 66(1), 1–16, doi: S0034-4257(98)00031-5, 1998.

Honda, M., Inoue, J., and Yamane, S.: Influence of low Arctic sea-ice minima on anomalously cold Eurasian winters. Geophys. Res. Lett., 36, L08707, doi:10.1029/2008GL037079, 2009.

Hong, S.-Y.: A new stable boundary-layer mixing scheme and its impact on the simulated East Asian summer monsoon, Q. J. R. Meteorol. Soc., 136, 1481–1496, doi:10.1002/qj.665, 2010.

Jackson, J. M., Carmack, E. C., McLaughlin, F. A., Allen, S. E. and Ingram, R.G.: Identification, characterization, and change of the near-surface temperature maximum in the Canada Basin, 1993–2008, J. Geophys. Res., 115, C05021, doi:10.1029/2009JC005265, 2010.

Jaiser, R. , Dethloff, K. , Handorf, D. , Rinke, A. and Cohen, J. : Planetary and synoptic scale feedbacks between tropospheric and sea ice cover changes in the Arctic, Tellus 64A, 11595., 2012.

Jakobson, E., Vihma, T., Palo, T., Jakobson, L., Keernik, H., and Jaagus, J.: Validation of atmospheric reanalyses over the central Arctic Ocean, Geophys. Res. Lett., 39, L10802, doi:10.1029/2012GL051591, 2012.

Janjic, Z.: Nonsingular implementation of the Mellor–Yamada level 2.5 scheme in the NCEP mesomodel, NCEP Office Note No. 437, National Centers for Environmental Prediction: Camp Springs, MD, USA, 2001.

Janssens-Maenhout,G., M. Crippa, D. Guizzardi, F. Dentener, M. Muntean, G. Pouliot, T. Keating, Q. Zhang, J. Kurokawa, R. Wankmüller, H. Denier van der Gon, Z. Klimont, G. Frost, S. Darras, and B. Koffi, M. Liu, J.J.P. Kuenen, HTAP_v2: a mosaic of regional and global emission gridmaps for 2008 and 2010 to study hemispheric transport of air pollution, Atmos. Chem. Phys. 15, 12867-12909, 2015.

Jiménez, P. A., and Dudhia, J.: Improving the representation of resolved and unresolved topographic effects on surface wind in the WRF model. J. Appl. Meteor. Climatol., 51, 300– 316, doi:10.1175/JAMC-D-11-084.1, 2012.

Katragkou, E., García-Díez, M., Vautard, R., Sobolowski, S., Zanis, P., Alexandri, G., Cardoso, R. M., Colette, A., Fernandez, J., Gobiet, A., Goergen, K., Karacostas, T., Knist, S., Mayer, S., Soares, P. M. M., Pytharoulis, I., Tegoulias, I., Tsikerdekis, A., and Jacob, D.: Regional climate hindcast simulations within EURO-CORDEX: evaluation of a WRF multi-physics ensemble, Geosci. Model Dev., 8, 603-618, doi:10.5194/gmd-8-603-2015, 2015.

Kleczek, M. A., Steeneveld, G., and Holtslag, A. A. M.: Evaluation of the Weather Research and Forecasting mesoscale model for GABLS3: impact of boundary-layer schemes, boundary conditions and spin-up, Bound.-Lay. Meteorol., 152, 213–243, 2014.

Jiao C., and Flanner, M.G.: Changing black carbon transport to the Arctic from present day to the end of 21st century, J. Geophys. Res. Atmos., 121, doi:10.1002/2015JD023964, 2016.

Jung, M., Reichstein, M., Ciais, P., Seneviratne, S. I., Sheffield, J., Goulden, M. L., Bonan, G., Cescatti, A., Chen, J., de Jeu, R., Dolman, A. J., Eugster, W., Gerten, D., Gianelle, D., Gobron, N., Heinke, J., Kimball, J., Law, B. E., Montagnani, L., Mu, Q., Mueller, B., Oleson, K., Papale, D., Richardson, A. D., Roupsard, O., Running, S., Tomelleri, E., Viovy, N., Weber, U., Williams, C., Wood, E., Zaehle, S., Zhang, K.: Recent decline in the global land evapotranspiration trend due to limited moisture supply. - Nature, 467, 7318, 951-954, 2010.

Lin, Y.–L., R. D. Farley, and H. D. Orville: Bulk Parameterization of the Snow Field in a Cloud Model, J. Climate Appl. Met., 22, 1065–1092, 1983.

Lindsay, R., Wensnahan, M., Schweiger, A., and Zhang, J.: Evaluation of Seven Different Atmospheric Reanalysis Products in the Arctic, Journal of Climate, 27, 2588–2606, doi:10.1175/JCLI-D-13-00014, 2014

Marelle, L., Thomas, J. L., Raut, J.-C., Law, K. S., Jalkanen, J.-P., Johansson, L., Roiger, A., Schlager, H., Kim, J., Reiter, A., and Weinzierl, B.: Air quality and radiative impacts of Arctic shipping emissions in the summertime in northern Norway: from the local to the regional scale, Atmos. Chem. Phys., 16, 2359-2379, doi:10.5194/acp-16-2359-2016, 2016.

Met Office: Met Office Integrated Data Archive System (MIDAS) Land and Marine Surface Stations Data (1853-current), NCAS British Atmospheric Data Centre,http://catalogue.ceda.ac.uk/, 2012.

Meier, W. N., Stroeve, J.C. and Fetterer, F.: Whiter Arctic sea ice? A clear signal of decline regionally, seasonally and extending beyond the satellite record, Annals of Glaciology, 46, 428-434, 2006.

Michalakes, J., Dudhia, J., Gill, D., Henderson, T., Klemp, J., Skamarock, W., and Wang, W.: The Weather Research and Forecast Model: Software Architecture and Performance, To appear in proceeding of the Eleventh ECMWF Workshop on the Use of High Performance Computing in Meteorology, 25–29 October 2004, Reading, U.K., Ed. George Mozdzynski, 2005.

Miguez-Macho, Li, G.,H. and Fan, Y.: Simulated water table and soil moisture climatology over North America. Bulletin of the American Meteorological Society 5: 663-672, doi: 10.1175/BAMS-89-5- 663, 2008.

Miguez-Macho, G. and Fan, Y.: The role of groundwater in the Amazon water cycle: 1. Influence on seasonal stream-flow, flooding and wetlands, J. Geophys. Res., 117, D15113, doi:10.1029/2012JD017539, 2012.

Misenis, C., and Zhang, Y.:An examination of sensitivity of WRF/Chem predictions to physical parameterizations, horizontal grid spacing, and nesting options, Atmospheric Research, 97, 315–334, doi:10.1016/j.atmosres.2010.04.005, 2010.

Mlawer, E., J., Steven. J. Taubman, Patrick. D. Brown, M. J. Iacono, and Clough, S. A.: Radiative transfer for inhomogeneous atmospheres: RRTM, a validated correlated–k model for the longwave, J. Geophys. Res., 102, 16663–16682, 1997.

Moore, G.W.K., Renfrew, I.A., Cassano J.J,: Greenland plateau jets. Tellus A 65: 17468, doi: 10.3402/tellusa.v65i0.17468, 2013.

NCAR,National Center for Atmospheric Research Staff (Eds), The Climate Data Guide: Arctic System Reanalysis (ASR), https://climatedataguide.ucar.edu/climate-data/arctic-system-reanalysis-asr, last modified 26 May 2015.

Niu, G.–Y., Z.-L. Yang, K. E. Mitchell, F. Chen, Ek, M. B., Barlage, M., Kumar, A.,, K. Manning, D. Niyogi, Rosero, E., Tewari, M. and Xia, Y.: The community Noah land surface model with multiparameterization options (Noah–MP): 1. Model description and evaluation with local–scale measurements, J. Geophys. Res., 116, D12109, 2011.

Nygård, T., T. Valkonen, T., and Vihma, T. : Characteristics of Arctic low-tropospheric humidity inversions based on radio soundings, Atmos. Chem. Phys., 14, 1959–1971, doi:10.5194/acp-14-1959-2014, 2014

Overland, J. E., and M. Wang: Large-scale atmospheric circulation changes are associated with the recent loss of Arctic sea ice, Tellus A., 62, 1–9, doi:10.1111/j.1600-0870.2009.00421, 2010.

Peckam, S. E., Grell, G. A., McKeen, S. A., Barth, M., Pfister,G., Wiedinmyer, C., Hewson, M., Freitas, S. R., Fast, J. D., Gustafson, W. I., Ghan, S. J., Zaveri, R., Easter, R. C., Barnard, J., Chapman, E., Schmitz, R., and Salzmann, M.: WRF/CHEM Version 3.4 User's Guide, available at: ruc.noaa.gov/wrf/WG11/Users guide.pdf, 2011.

Petoukhov, V., and V. A. Semenov: A link between reduced Barents-Kara sea ice and cold winter extremes over northern continents, J. Geophys. Res., 115, D21111, doi:10.1029/2009JD013568, 2010.

Pino, D., Jonker, H., Vilà-Guerau De Arellano, J., and Dosio, A.: Role of Shear and the Inversion Strength During Sunset Turbulence Over Land: Characteristic Length Scales, Bound.-Lay. Meteorol. 121, 537–556, doi:10.1007/s10546-006-9080-6, 2016.

Randerson, J.T., van der Werf, G.R., Giglio, L. Collatz, G.J. and Kasibhatla, P.S.: Global Fire Emissions Database, Version 4, (GFEDv4). ORNL DAAC, Oak Ridge, Tennessee, USA. http://dx.doi.org/10.3334/ORNLDAAC/1293, 2015.

Richards, L.A.: Capillary conduction of liquids through porous mediums. Physics 1 (5): 318–333. doi:10.1063/1.1745010, 1931.

Rinke, A., A. H. Lynch, and K. Dethloff: Intercomparison of Arctic regional climate simulations: Case studies of January and June 1990, J. Geophys. Res., 105(D24), 29669–29683, doi:10.1029/2000JD900325, 2000.

Santos-Alamillos, F. J., Pozo-Vázquez, D., Ruiz-Arias, J. A., Lara-Fanego, V., and TovarPescador, J.: Analysis of WRF model wind estimate sensitivity to physics parameterization choice and terrain representation in Andalusia (Southern Spain), J. Appl. Meteorol. Clim., 25 52, 1592–1609, doi:10.1175/JAMC-D-12-0204.1, 2013.

Sahsamanoglou, H. S.: A contribution to the study of the action centers in the North Atlantic, Int. J. Climatol., 10, 247-261, 1990.

Screen, J. A., and Simmonds, I.: The central role of diminishing sea ice in recent Arctic temperature amplification, Nature, 464, 1334-1337, 2010.

Schnell, R.C., ed.: Arctic Haze Special Issue, Geophys. Res. Lett., 11, 359-472, 1984.

Schell B., I.J. Ackermann, H. Hass, F.S. Binkowski, and A. Ebel: Modeling the formation of secondary organic aerosol within a comprehensive air quality model system, Journal of Geophysical research, 106, 28275-28293, 2011.

Schmittner, A., Yoshimori, M., Weaver, A.J.: Instability of glacial climate in a model ofthe ocean–atmosphere–cryosphere system. Science 295, 1493–1498, 2002.

Seager, R., Y. Kushnir, J. Nakamura, M. Ting, and N. Naik: Northern hemisphere winter snow anomalies: ENSO, NAO and the winter of 2009/10, Geophys. Res. Lett., 37, L14703, doi:10.1029/2010GL043830, 2010.

Skamarock, W. C., J. B. Klemp, J. Dudhia, D. O. Gill, D. M. Barker, W. Wang, and J. G. Powers: A description of the Advanced Research WRF Version 2. NCAR Tech Notes-468+STR, 2005.

Serreze, M. C., Walsh, J. E., Chapin, F. S., III, Osterkamp, T., Dyurgerov, M., Romanovsky, V., Oechel, W. C., Morison, J., Zhang, T. and Barry, R. G.: Observational evidence of recent change in the northern high-latitude environment, Climatic Change, 46(1-2), 159–207, 2000.
Stohl, A.:Characteristics of atmospheric transport into the Arctic troposphere, J. Geophys. Res., 111, D11306, 2006.

Taylor, K. E.: Summarizing multiple aspects of model performance in a single diagram, J. Geophys. Res., 106, 7183, doi:10.1029/2000JD900719, 2001.

Trenberth, K. E., Koike, T., and Onogi, K.,: Progress and Prospects for Reanalysis for Weather and Climate, Eos Trans. AGU, 89(26), 234–235, doi:10.1029/2008EO260002, 2008.

Trenberth, K. E., and Fasullo, J. T.: Climate extremes and climate change: The Russian heat wave and other climate extremes of 2010, J. Geophys. Res., 117, D17103, doi:10.1029/2012JD018020, 2012.

Vihma, T., Pirazzini, R., Fer, I., Renfrew, I. A., Sedlar, J., Tjernström, M., Lüpkes, C., Nygård, T., Notz, D., Weiss, J., Marsan, D., Cheng, B., Birnbaum, G., Gerland, S., Chechin, D., and Gascard, J. C.: Advances in understanding and parameterization of small-scale physical processes in the marine Arctic climate system: a review, Atmos. Chem. Phys., 14, 9403-9450, doi:10.5194/acp-14-9403-2014, 2014.

Wang, Q., Jacob, D. J., Fisher, J. A., Mao, J., Leibensperger, E. M., Carouge, C. C., Le Sager, P., Kondo, Y., Jimenez, J. L., Cubison, M. J., and Doherty, S. J.: Sources of carbonaceous aerosols and deposited black carbon in the Arctic in winter-spring: implications for radiative forcing, Atmos. Chem. Phys., 11, 12453-12473, doi:10.5194/acp-11-12453-2011, 2011.

Warneke, C., Bahreini, R., Brioude, J., Brock, C. A., De Gouw, J., Fahey, D. W., Froyd, K. D., Holloway, J. S., Middlebrook, A., Miller, L., Montzka, S., Murphy, D. M., Peischl, J.,. Ryerson, T. B, Schwarz, J. P., Spackman, J. R., and Veres, P.: Biomass burning in Siberia and Kazakhstan as an important source forhaze over the Alaskan Arctic in April 2008, Geophys. Res. Lett., 36, L02813, doi:10.1029/2008GL036194, 2009.

Atmos. Chem. Phys. Discuss., doi:10.5194/acp-2016-942, 2016
Manuscript under review for journal Atmos. Chem. Phys.
Published: 24 November 2016

Atmospheric Chemistry and Physics Discussions

Wehner M., Smith, R., Bala, G. and Duffy, P.: The effect of horizontal resolution on simulation of very extreme US precipitation events in a global atmosphere model, Clim. Dyn., 34, 241–247, 2010.

Wesslén, C., Tjernström, M., Bromwich, D. H., de Boer, G., Ekman, A. M. L., Bai, L.-S., and Wang, S.-H.: The Arctic summer atmosphere: an evaluation of reanalyses using ASCOS data, Atmos. Chem. Phys., 14, 2605-2624, doi:10.5194/acp-14-2605-2014, 2014.

Wiedinmyer, C., Akagi, S. K., Yokelson, R. J., Emmons, L. K., Al-Saadi, J. A., Orlando, J. J., and Soja, A. J.: The Fire INventory from NCAR (FINN): a high resolution global model to estimate the emissions from open burning, Geosci. Model Dev., 4, 625-641, doi:10.5194/gmd-4-625-2011, 2011.

Wright, C.K., K.M. de Beurs and G.M. Henebry: Land surface anomalies preceding the 2010 Russian heat wave and a link to the North Atlantic oscillation. Environmental Research Letters, 9, 2010.

Yang, Z.-L., Niu, G.-Y., Mitchell, K. E., Chen, F., Ek, M. B., Barlage, M., Longuevergne, L., Manning, K., Niyogi, D., Tewari, M., and Xia, Y.: The community Noah land surface model with multiparameterization options (Noah-MP): 2. Evaluation over global river basins, J. Geophys. Res., 116, D12110,doi:10.1029/2010JD015140, 2011.

Atmos. Chem. Phys. Discuss., doi:10.5194/acp-2016-942, 2016
Manuscript under review for journal Atmos. Chem. Phys.
Published: 24 November 2016

Atmospheric Chemistry and Physics Discussions
Open Access
EGU

List of Tables

Table 1. Model configuration and sensitivity experiments.

a) Model physical set up	
Model	WRF (ARW) version 3.7.1
Simulation period	Years 2008-2012 Winter: January, February, March (JFM) Summer: July, August, September (JAS)
Domain	270 X 252 grid points (175°W-175°E and 45°N-90°N)
Projection	Polar stereographic, center at 70°N, 40°E
Horizontal Resolution	15 km x 15 km
Vertical levels	30 σ-levels (11 levels below σ = 0.9)
Physical configuration[a]:	
Shortwave radiation:	Goddard scheme
Longwave radiation:	RRTM scheme
Cloud microphysics:	Purdue Lin scheme
Cumulus scheme:	Grell-3D ensemble scheme
PBL scheme:	Yonsei University Scheme (YSU)
Surface Layer:	MM5 Similarity
Land Surface Model (LSM):	∗ Unified Noah ∗ NoahMP
Data for initialization and lateral boundary conditions:	∗ ERA-Interim ∗ Arctic System Reanalysis (ASR)
b) Experiments and Description:	
Noah_ecmwf	Noah LSM + ERA-Interim reanalysis
NoahMP_ecmwf	NoahMP LSM + ERA-Interim reanalysis
Noah_asr	Noah LSM + ASR reanalysis
NoahMP_asr	NoahMP LSM + ASR reanalysis

[a] See text for references
∗ Sensitivity analyses

Atmos. Chem. Phys. Discuss., doi:10.5194/acp-2016-942, 2016
Manuscript under review for journal Atmos. Chem. Phys.
Published: 24 November 2016

Table 2. Model set up for the WRF-Chem runs with chemistry and aerosols (physical parameterizations and domain settings as for the meteorology-only WRF runs given in Table 1).

Model	**WRF-Chem version 3.7.1**
Simulation period	April 2008 July 2008 April 2009 July 2010
Chemistry	RADM2+CMAQ scheme
Aerosols	MADE/SORGAM scheme
Dust	GOCART on-line dust emissions (AFWA modification)
Input data	
Boundary conditions chemistry	MOZART (Global CTM)
Anthropogenic emissions	EDGAR HTAP v2.2 (resolution 0.1°x0.1°)
Fire emissions	NCAR FINN v1.0
Biogenic emissions	MEGAN (online)
Time profiles	Yearly cycle (monthly data)

Atmos. Chem. Phys. Discuss., doi:10.5194/acp-2016-942, 2016
Manuscript under review for journal Atmos. Chem. Phys.
Published: 24 November 2016

Atmospheric Chemistry and Physics Discussions
Open Access

1019 **Table 3. List of stations used for model evaluation (in bold, stations located north of 66°N).**

Station	Code	Latitude	Longitude	WMO
1. Krenkelja, RU *	**KRE**	80.64 °N	58.049 °E	20046
2. Ostrov Golomjannyj RU	**GOL**	79.55 °N	90.617 °E	N/A
3. Ny-Alesund, NO	**ALE**	78.92 °N	11.93 °E	01004
4. Danmarkshavn GRE	**DAN**	76.76 °N	18.66 °W	04320
5. Ostrov Dikson, RU	**DIK**	73.50 °N	80.42 °E	20674
6. Popova RU *	**POP**	73.33 °N	70.05 °E	N/A
7. Malye Karmakuly, RU	**MAL**	72.38 °N	52.73 °E	20744
8. Murmansk, RU	**MUR**	68.98 °N	33.12 °E	22113
9. Sojna RU	**SOJ**	67.87 °N	44.17 °E	22271
10. Narian Mar, RU	**NAR**	67.65 °N	53.02 °E	23205
11. Bodo, NO	**BOD**	67.26 °N	14.366 °E	01152
12. Kandalaksa, RU	**KAN**	67.15 °N	32.35 °E	22217
13. Sale-Khard , RU	**SAL**	66.53 °N	66.66 °E	23330
14. Turukhansk, RU	TUR	65.78 °N	87.95 °E	23472
15. Lulea-Kallax, SWE	LUL	65.55 °N	22.13 °E	02185
16. Arhangel'Sk,RU	ARH	64.58 °N	40.5 °E	22550
17. Orland, NO	ORL	63.70 °N	9.60 °E	01241
18. Timra, SWE	TIM	62.51 °N	17.45 °E	02365
19. Syktyvkar, RU	SYK	61.66 °N	50.85 °E	23804
20. Samarovo, RU	SAM	60.97 °N	69.07 °E	23933
21. Jokioinen, FIN	JOK	60.82 °N	23.50 °E	02963
22. Ivdel, RU	IVD	60.68°N	60.43 °E	23921
23. Leningrad, RU	LEN	59.95 °N	30.70 °E	26063
24. Moscow, RU	MOC	55.75 °N	37.57 °E	27612

1020 * No radiosonde data for analyzed period
1021
1022

Atmos. Chem. Phys. Discuss., doi:10.5194/acp-2016-942, 2016
Manuscript under review for journal Atmos. Chem. Phys.
Published: 24 November 2016

Atmospheric Chemistry and Physics
Discussions
Open Access
EGU

Table 4. Biases and RMS error of 6-hourly values from the ERA-Interim and ASR reanalyses and the 4 WRF experiments compared against surface meteorological observations from AWS.

	Stations above **66°N** *stations*				*Stations below* **66°N**			
Temperature (°C)	***FMA***		***JAS***		***FMA***		***JAS***	
	Bias	**RMS**	**Bias**	**RMS**	**Bias**	**RMS**	**Bias**	**RMS**
Reanalysis								
ERA-Interim	0,40	2,40	-0,25	1,81	-0,12	1,78	-0,10	1,81
ASR	0,18	1,53	-0,25	1,06	-0,28	1,18	-0,19	0,85
WRF Experiments								
noah_ecmwf	-0,70	6,08	-1,74	3,15	-3,21	5,80	-1,64	2,94
noahMP_ecmwf	0,53	6,19	-1,57	3,11	-1,23	5,62	-1,03	2,99
noah_asr	0,83	6,79	-0,87	3,09	-1,77	5,75	-0,99	3,20
noahMP_asr	1,99	6,96	-0,84	3,05	-0,01	5,88	-0,59	3,15
Wind Speed (m/s)	**FMA**		**JAS**		**FMA**		**JAS**	
	Bias	**RMS**	**Bias**	**RMS**	**Bias**	**RMS**	**Bias**	**RMS**
Reanalysis								
ERA-Interim	0,81	2,57	0,38	1,89	0,78	2,01	0,90	1,85
ASR	-0,17	1,99	0,02	1,43	-0,32	1,63	-0,15	1,38
WRF Experiments								
noah_ecmwf	0,74	3,31	0,63	2,78	0,84	2,42	0,94	2,19
noahMP_ecmwf	0,55	3,26	0,38	2,58	0,61	2,23	0,61	1,99
noah_asr	0,89	3,75	0,67	2,91	0,79	2,54	0,93	2,22
noahMP_asr	0,70	3,66	0,50	2,83	0,62	2,41	0,61	2,04
SLP (milibars)	**FMA**		**JAS**		**FMA**		**JAS**	
	Bias	**RMS**	**Bias**	**RMS**	**Bias**	**RMS**	**Bias**	**RMS**
Reanalysis								
ERA-Interim	-0,06	0,56	-0,01	0,49	-0,03	0,46	-0,09	0,41
ASR	-0,59	0,63	-0,24	0,52	-0,43	0,60	-0,08	0,42
WRF Experiments								
noah_ecmwf	0,28	5,79	-0,19	4,94	0,57	4,65	-0,39	3,38
noahMP_ecmwf	0,12	5,74	-0,11	4,20	-0,03	4,56	-0,54	2,93
noah_asr	-2,69	7,80	-1,45	5,57	-0,99	5,82	-0,59	3,73
noahMP_asr	-2,93	7,89	-1,17	5,51	-1,68	5,64	-0,37	3,43

Atmos. Chem. Phys. Discuss., doi:10.5194/acp-2016-942, 2016
Manuscript under review for journal Atmos. Chem. Phys.
Published: 24 November 2016

Table 5. Mean vertical profiles statistics: biases and RMS for the ERA-Interim and ASR renalyses and the 4 WRF experiments against radiosonde observations from the IGRA database.

	Stations above 66°N				*Stations below* 66°N			
Temperature (°C)	***FMA***		***JAS***		***FMA***		***JAS***	
	Bias	**RMS**	**Bias**	**RMS**	**Bias**	**RMS**	**Bias**	**RMS**
Reanalysis								
ERA-Interim	1,15	1,50	0,42	0,58	1,73	2,10	0,33	0,66
ASR	0,46	0,73	-0,58	1,49	0,73	0,97	-1,58	2,47
WRF Experiments								
noah_ecmwf	0,26	0,92	0,27	0,97	0,06	1,19	0,27	0,83
noah_asr	0,51	1,43	0,43	1,21	0,82	1,35	0,58	0,91
noahMP_asr	1,07	2,04	0,43	1,24	1,60	1,91	0,78	1,06
noahMP_ecmwf	0,89	1,33	0,40	1,01	0,97	1,34	0,54	0,89
Wind Speed (m/s)	**FMA**		**JAS**		**FMA**		**JAS**	
	Bias	**RMS**	**Bias**	**RMS**	**Bias**	**RMS**	**Bias**	**RMS**
Reanalysis								
ERA-Interim	-0,67	1,00	-0,42	0,67	-0,34	0,92	-0,36	0,73
ASR	-0,45	0,82	0,00	0,71	-0,26	0,645	-0,10	0,84
WRF Experiments								
noah_ecmwf	0,97	1,55	0,52	1,01	0,89	1,388	0,40	1,04
noah_asr	1,34	1,94	0,55	1,11	0,93	1,493	0,38	1,10
noahMP_asr	1,18	1,82	0,53	1,03	0,68	1,351	0,19	1,04
noahMP_ecmwf	0,85	1,47	0,33	0,86	0,47	1,176	0,31	1,01
% Humidity	**FMA**		**JAS**		**FMA**		**JAS**	
	Bias	**RMS**	**Bias**	**RMS**	**Bias**	**RMS**	**Bias**	**RMS**
Reanalysis								
ERA-Interim	7,05	8,94	2,24	4,41	5,71	8,07	1,76	4,06
ASR	-2,15	4,15	1,22	3,78	-0,64	3,28	2,75	5,38
WRF Experiments								
noah_ecmwf	-3,92	7,43	-0,22	5,97	0,20	7,13	0,07	6,77
noah_asr	-1,54	8,00	1,69	6,56	0,08	6,96	1,1	5,92
noahMP_asr	-3,58	8,93	1,84	6,78	-3,24	6,64	-0,4	5,73
noahMP_ecmwf	-5,96	8,38	-0,77	5,84	-3,56	6,70	-1,63	5,99

Atmos. Chem. Phys. Discuss., doi:10.5194/acp-2016-942, 2016
Manuscript under review for journal Atmos. Chem. Phys.
Published: 24 November 2016

Atmospheric Chemistry and Physics Discussions

List of Figures

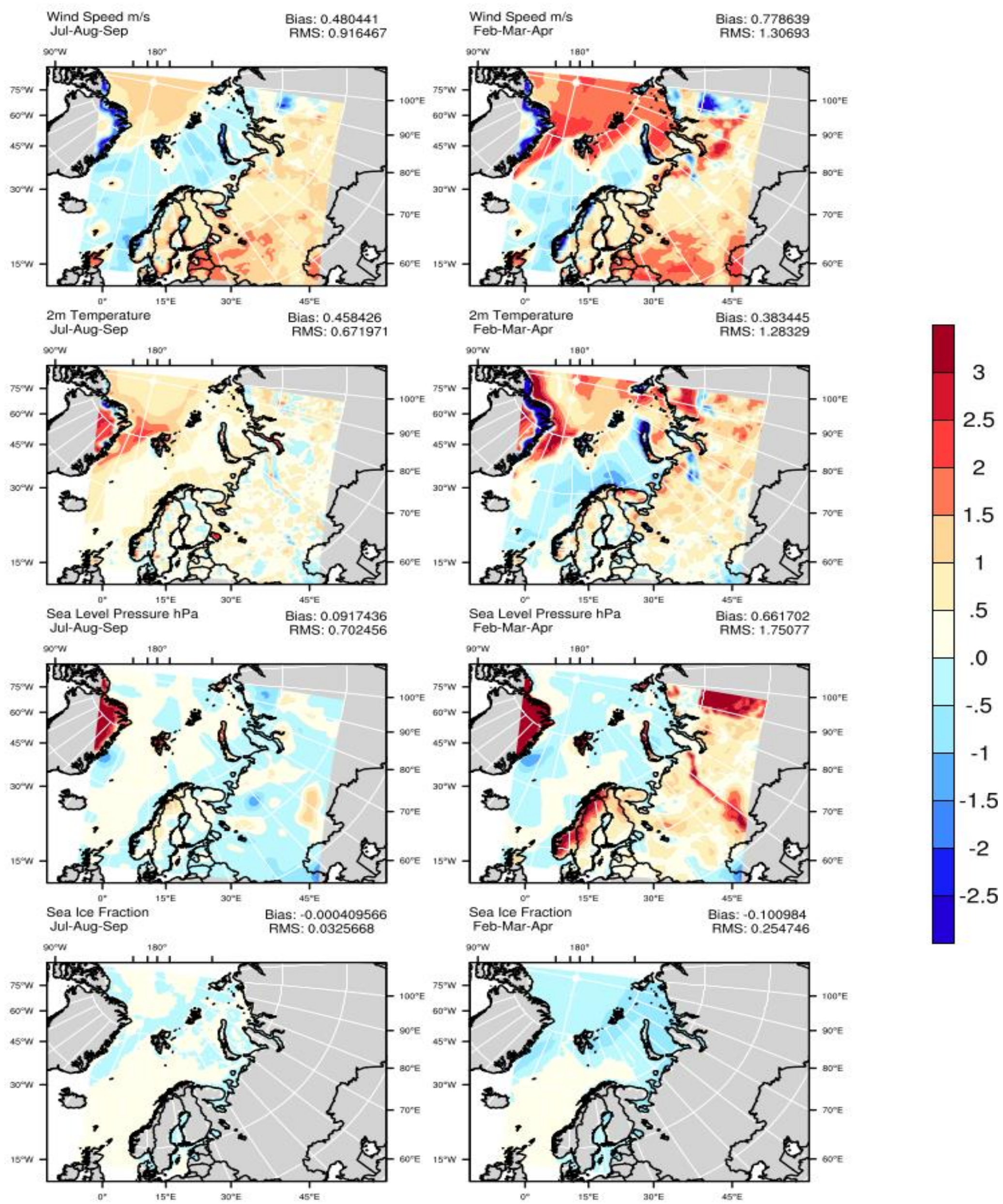

Figure 1. Differences between the ERA-Interim and the ASR reanalyses for a) 10m wind speed in m/s, b) 2m temperature in °C, c) sea level pressure in hPa, and d) sea ice in fractional units for summer (JAS; left column) and winter (FMA; right column) averaged over five seasons (2008-2012). The root mean square (RMS) error and mean bias are given above each panel as a measure of the differences between the two reanalyes.

Atmospheric Chemistry and Physics
Open Access
Discussions

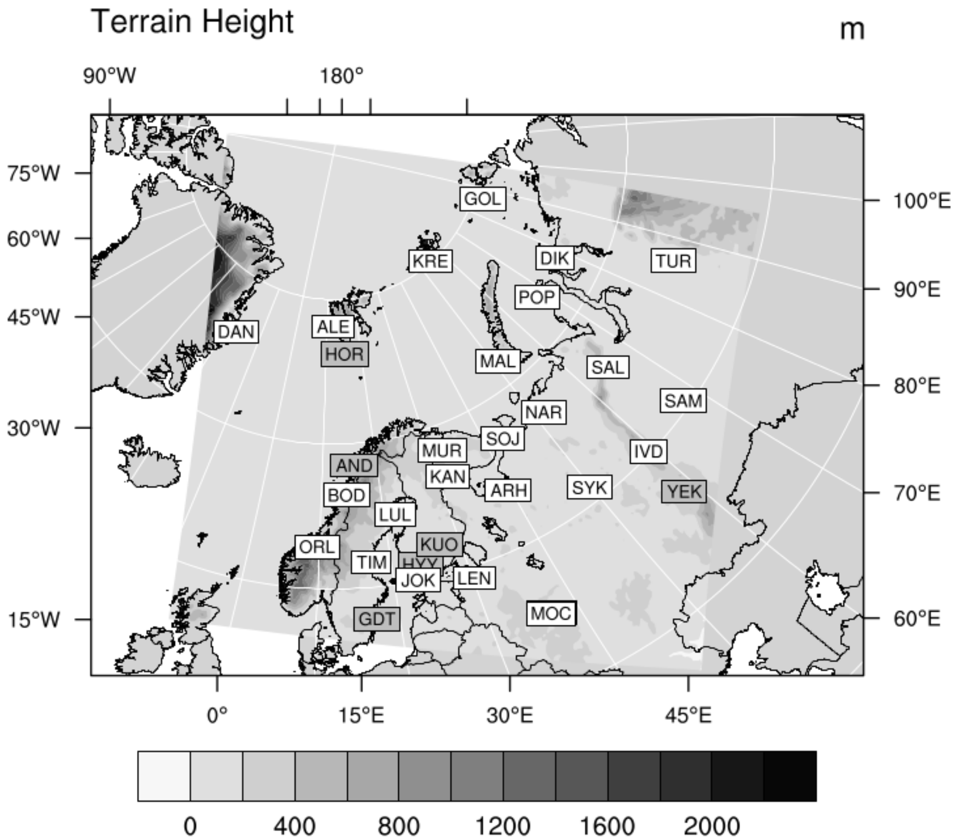

Figure 2. Model domain, topographic height (m), and location of the observational stations from WMO (white labels) and AERONET (grey labels) used for the model evaluation

Atmos. Chem. Phys. Discuss., doi:10.5194/acp-2016-942, 2016
Manuscript under review for journal Atmos. Chem. Phys.
Published: 24 November 2016

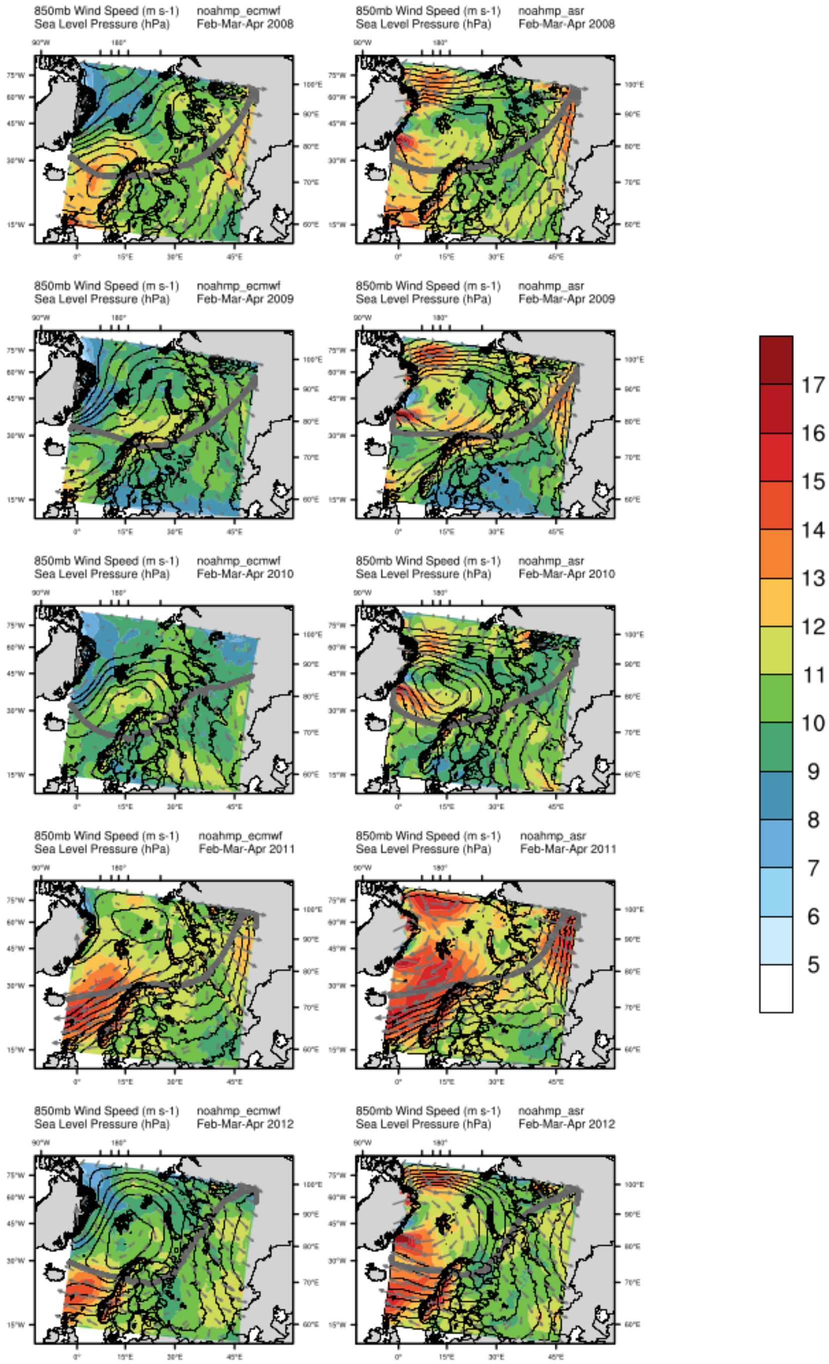

Figure 3. Modeled 3-month means of the sea level pressure and 850 hPa winds for winter months (February, March, April) from 2008-2012. Left column represents experiment *noahmp_ecmwf* and right column for experiment *noahmp_asr*. Solid lines are isobars (contours from 1004-1020 hPa), color shading is wind speed at 850 hPa in ms^{-1} and gray arrows represent wind direction. The maximum gradient in geopotential height at 500 hPa (thick gray contour line) is used here as an approximation of the Arctic dome.

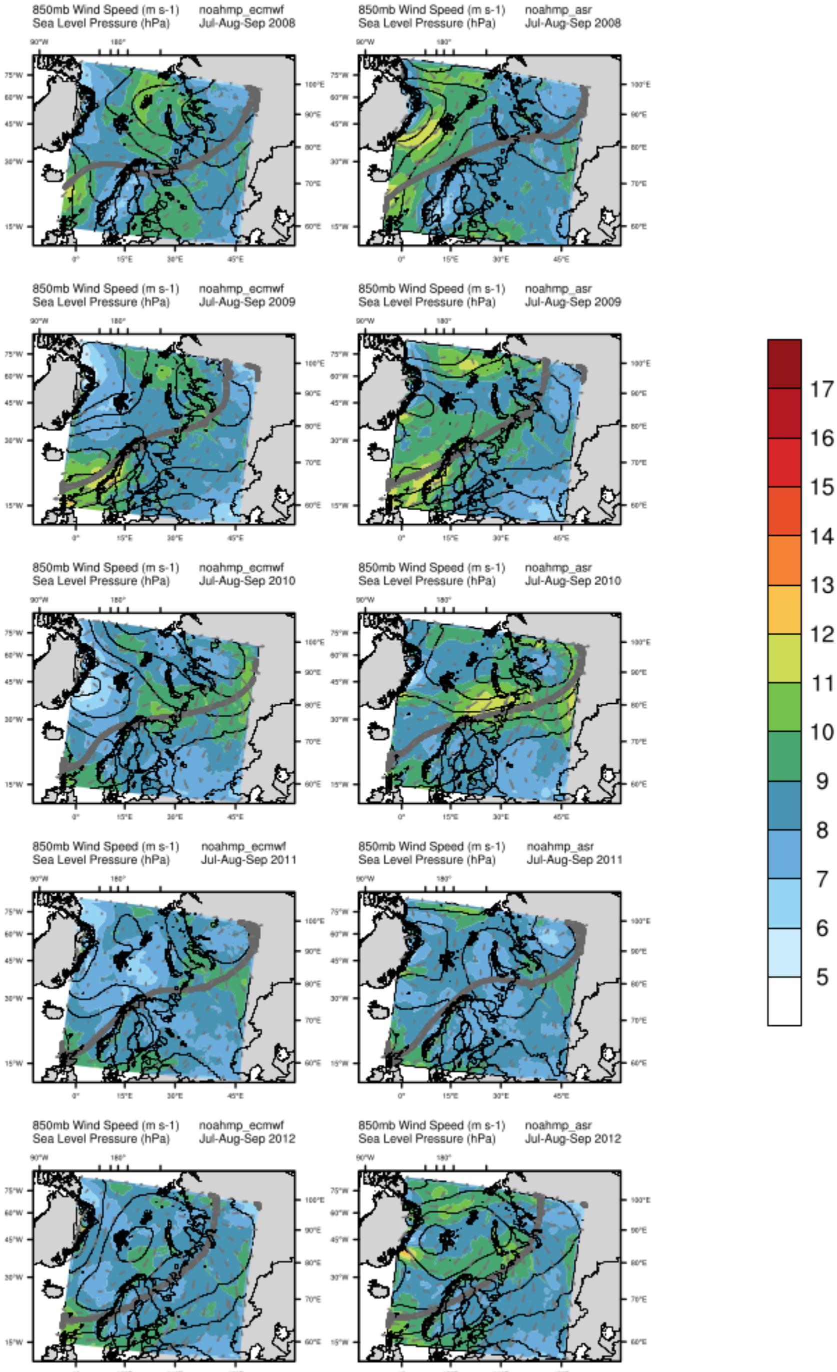

1058

1059 **Figure 4. Same as Figure 3 but for summer months (July, August, September).**

1060

Atmos. Chem. Phys. Discuss., doi:10.5194/acp-2016-942, 2016
Manuscript under review for journal Atmos. Chem. Phys.
Published: 24 November 2016

Atmospheric Chemistry and Physics
Discussions

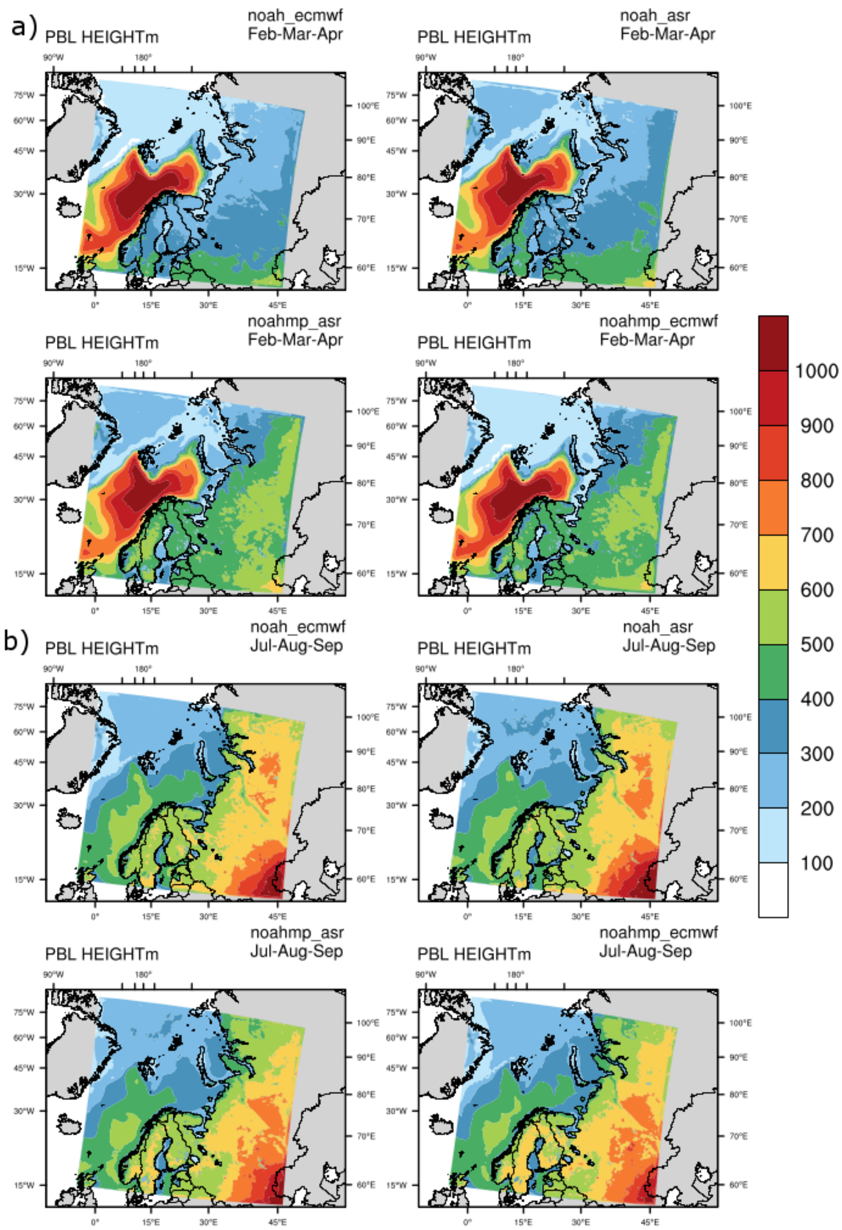

Figure 5. Five year averages of the planetary boundary layer height for a) winter months (February, March and April) and for b) summer months (July, August and September) from the four meteorology-only WRF experiments (*noah_ecmwf*, *noah_asr*, *noahmp_ecmwf*, and *noahmp_asr*).

Atmospheric Chemistry and Physics
Discussions

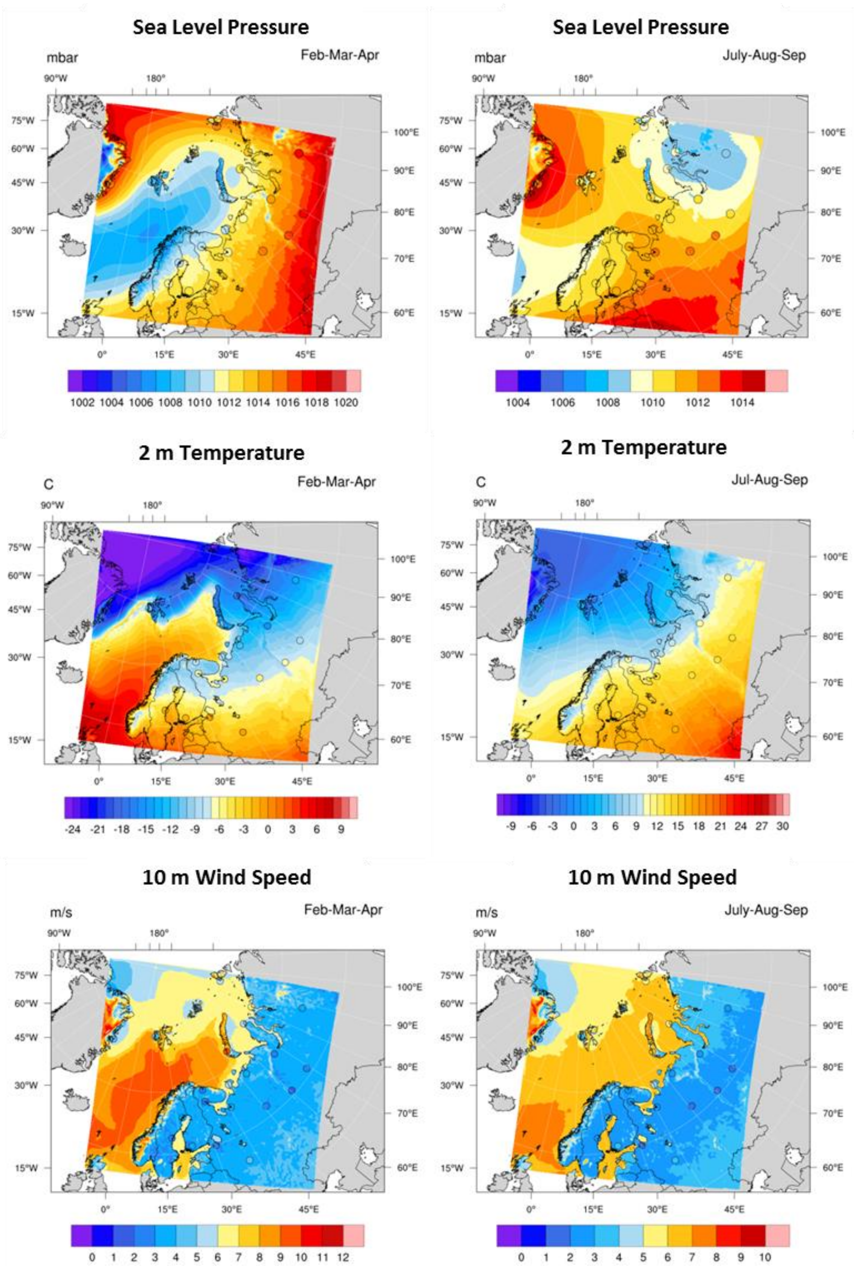

Figure 6. Mean modeled spatial distribution (colored fields) and station observations (colored circles) of sea level pressure (hPa), 2m temperature (ºC) and 10m wind speed (m/s) from from the meteorological experiment noahmp_ecmwf for winter (left column) and summer months (right column).

Atmospheric Chemistry and Physics
Open Access
Discussions

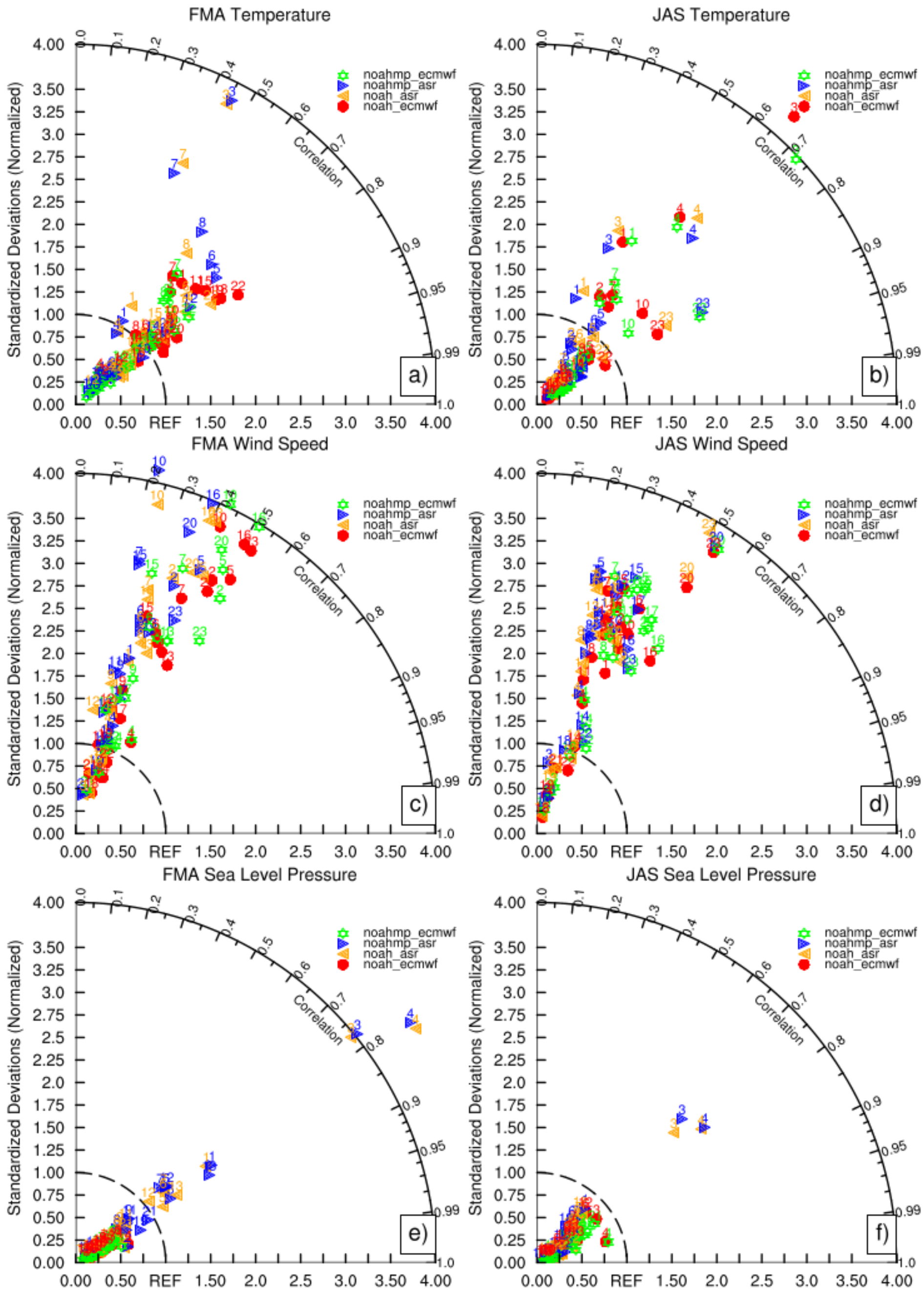

Figure 7. Taylor diagrams comparing surface observations from 22 stations with the four meteorology-only model experiments calculated from time series of daily means over the five year period 2008-2012 for the winter months (FMA; left column) and summer (JAS; right column)for 2m temperature (a-b), 10m wind speed (c- d) and sea level pressure (e-f).

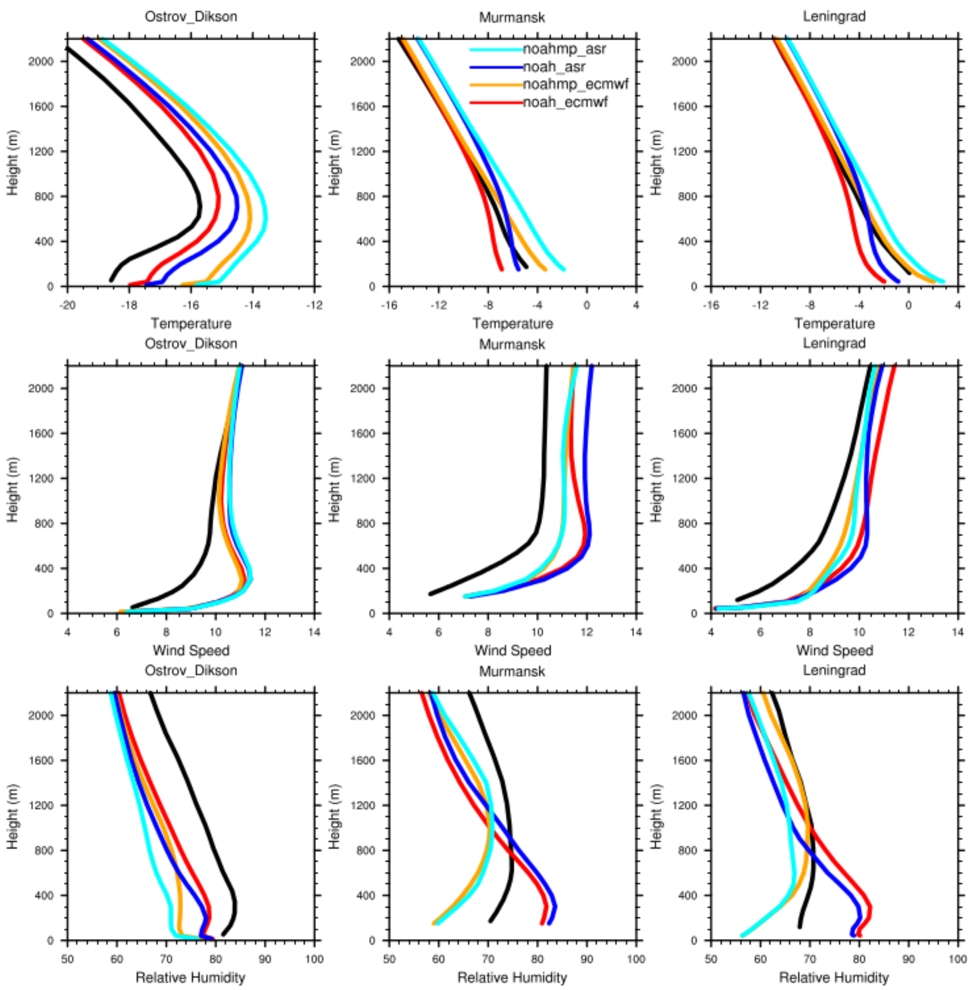

Figure 8. Radiosonde and modeled mean profiles at midday readings from the 4 meteorology-only WRF model runs compared with radiosonde measurements (black line) at three selected stations for winter months (Febrero, March and April) for temperature in °C (first row) wind speed in m/s (middle row) and relative humidity in % (last row).

Atmos. Chem. Phys. Discuss., doi:10.5194/acp-2016-942, 2016
Manuscript under review for journal Atmos. Chem. Phys.
Published: 24 November 2016

Atmospheric Chemistry and Physics
Open Access
Discussions

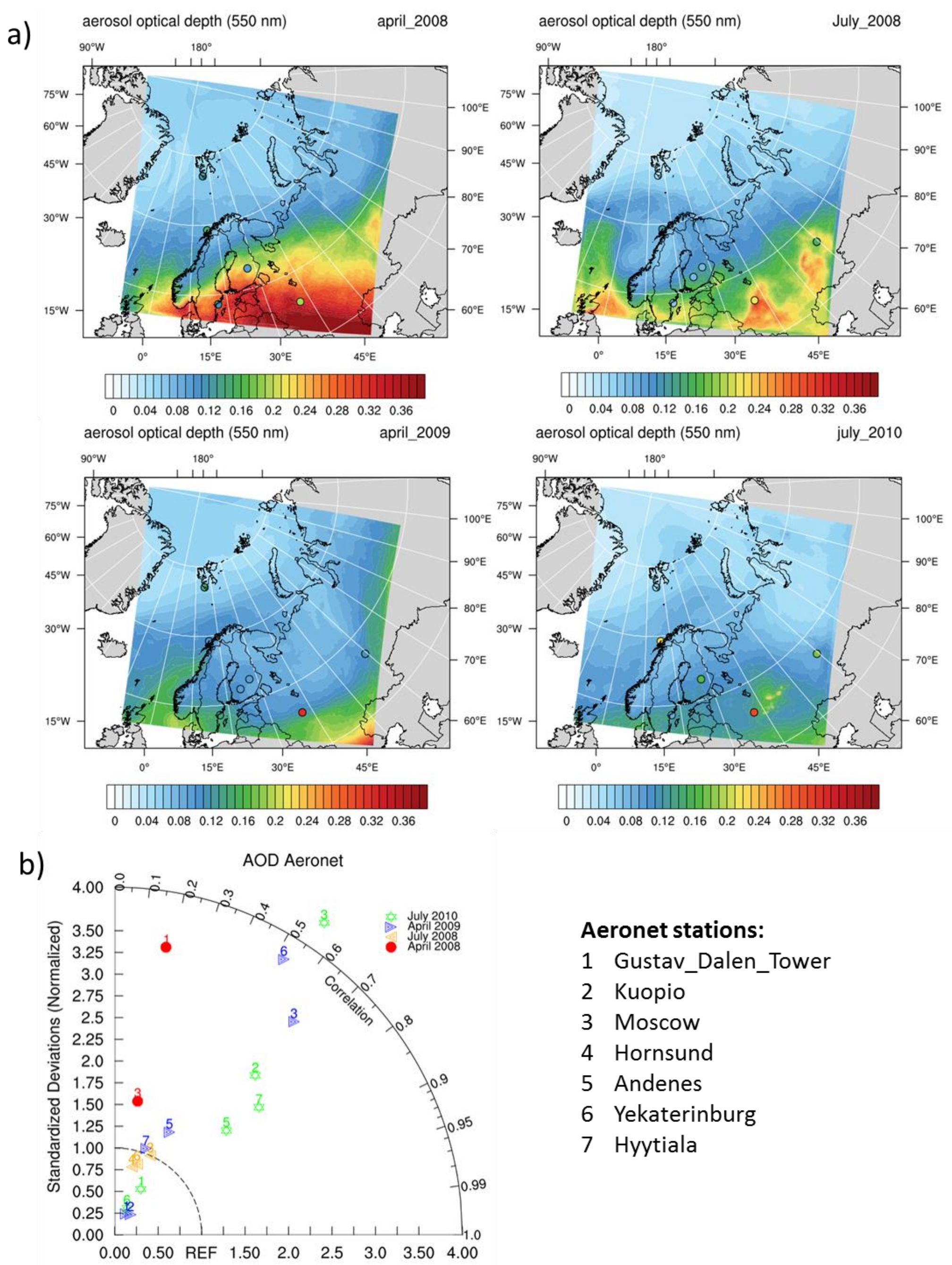

Figure 9. Comparison of the modeled mean AOD from the experiment with WRF-Chem and AOD from Aeronet observations, a) spatial distribution (colored fields) and AERONET mean observations (colored circles) and b)Taylor diagrams displaying a comparison between timeseries of observational AOD at different Aeronet stations versus modeled AOD.

Atmos. Chem. Phys. Discuss., doi:10.5194/acp-2016-942, 2016
Manuscript under review for journal Atmos. Chem. Phys.
Published: 24 November 2016

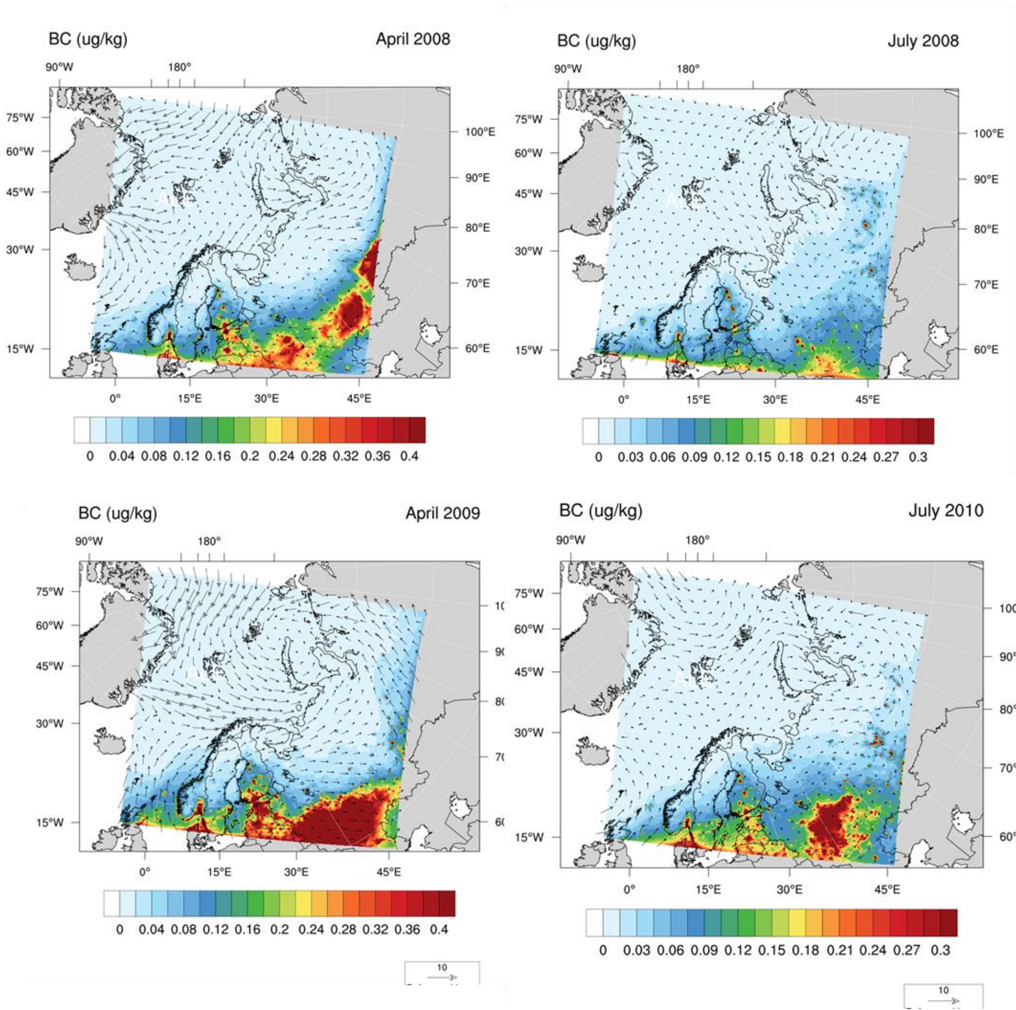

Figure 10. Simulated monthly mean BC concentrations near the surface (colored fields) and 10m wind (arrows) from WRF-Chem for April 2008, July 2008, April 2009 and July 2010.

Atmos. Chem. Phys. Discuss., doi:10.5194/acp-2016-942, 2016
Manuscript under review for journal Atmos. Chem. Phys.
Published: 24 November 2016

Atmospheric Chemistry and Physics
Discussions

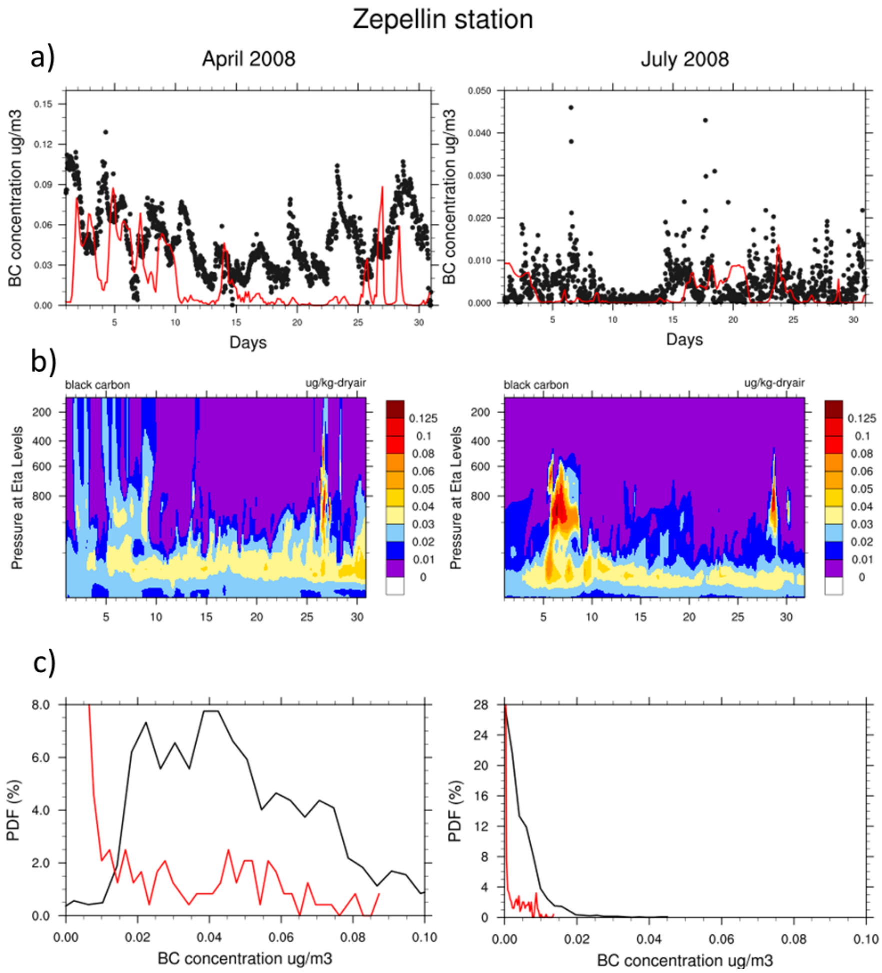

Figure 11. Time series of April and July 2008 a) modeled (red line) and observed (black dots) surface BC concentrations at Zeppelin station in Ny-Ålesund, b) vertical distribution of modeled BC and c) probability density function of BC calculated from hourly values of BC concentrations for the studied periods for the model (red line) and observations (black line).